Nádia Alexandra Esteves Santos

Síntese e avaliação de novos pirazóis, glicosilpirazóis e rutenopirazóis para atividade antioxidante e antitumoral

Synthesis and evaluation of new pyrazoles, glycosylpyrazoles and rutheniumpyrazoles for antioxidant and antitumoral activity

Nádia Alexandra Esteves Santos

Síntese e avaliação de novos pirazóis, glicosilpirazóis e rutenopirazóis para atividade antioxidante e antitumoral

Synthesis and evaluation of new pyrazoles, glycosylpyrazoles and rutheniumpyrazoles for antioxidant and antitumoral activity

Dissertação apresentada à Universidade de Aveiro para cumprimento dos requisitos necessários à obtenção do grau de Mestre em Biotecnologia, ramo Molecular, realizada sob a orientação científica da Doutora Susana Braga, Investigadora do Departamento de Química da Universidade de Aveiro, e co-orientação da Doutora Vera Silva, Investigadora do Departamento de Química da Universidade de Aveiro.

o júri

presidente
Professor Doutor João Filipe Colardelle da Luz Mano
Professor Catedrático do Departamento de Química da Universidade de Aveiro

orientador
Doutora Susana Isabel Fonseca de Almeida Santos Braga
Equiparada a Investigadora Associada, Departamento de Química, Universidade de Aveiro

arguente
Doutor Leandro Miguel de Oliveira Lourenço
Investigador Convidado, Departamento de Química, Universidade de Aveiro

agradecimentos

Gostaria de começar por agradecer às minhas orientadoras, a Dr.ª Susana Braga e a Dr.ª Vera Silva. Um muito obrigada pela paciência, pelo acompanhamento, força, confiança e otimismo no meu trabalho e assim me fazerem crescer não só como profissional, mas também como pessoa.

Obrigada à Universidade de Aveiro e principalmente ao Departamento de Química, pelos excelentes professores que nos ensinam ao longo de toda esta etapa.

Obrigada aos amigos que fiz nesta academia, por todas as gargalhadas e por todas as coisas que passamos juntos. Aos amigos de longa data também: Nádia, Diogo, Ângela, entre outros, muito obrigada pelo vosso apoio incondicional.

Obrigada a todos os meus familiares por todo o apoio ao longo destes anos e por falarem sempre de mim com orgulho na sua voz.

Deixo a última parte destes agradecimentos dedicada às pessoas mais importantes da minha vida: a minha mãe, pai, irmão e o meu namorado. Obrigada mãe por seres a minha fonte de força, a minha melhor amiga. Obrigada pai por seres a minha fonte de inspiração, a pessoa que tanto admiro. Obrigada aos dois pelo esforço e trabalho para me darem esta oportunidade. Obrigada a ti, mano mais novo, por seres um dos homens da minha vida e fonte de força. Já não sou apenas eu que te protejo. Tu proteges-me imenso. Por fim, obrigada ao amor da minha vida, Rodolfo. Obrigada por teres aparecido na minha vida. Obrigada pelas vezes que suportas as minhas ansiedades, os meus ataques de desespero sem nunca te queixares... Obrigada por estares sempre aqui. Amo-vos muito a todos.

Aqui começa uma nova etapa... Obrigada a todos que fizeram parte deste capítulo.

palavras- Chave

Cancro, pirazóis, complexos de ruténio, antitumoral, antioxidante, anti-inflamação

resumo

O cancro é a segunda maior razão de morte em Portugal, a seguir às doenças cardiovasculares. A quimioterapia continua a ser o tratamento mais utilizado e eficaz, no entanto o intervalo onde a dose é eficiente e ao mesmo tempo segura ainda é muito pequeno, podendo ser tóxico para o organismo do paciente. Dessa forma, a procura de novos agentes antitumorais eficientes e seguros tem sido crucial, tendo os pirazóis e os complexos de ruténio (II) um papel muito importante. Vários compostos contendo o anel de pirazol nas suas estruturas já demonstraram grande poder antitumoral ao inibirem enzimas cinases, tais como as aurosa cinases e as cinases dependentes de ciclina, ao induzirem a apoptose e até agindo como agentes citotóxicos contra linhas celulares tumorais. Os complexos de ruténio, por sua vez, contribuem para uma ação antitumoral mais seletiva, por terem propriedades redox ou pela incorporação de ligandos lábeis que criam locais de ligação a biomoléculas.

Neste trabalho pretende-se sintetizar novos derivados de pirazol, proceder à sua glicosilação e ligação com um complexo de ruténio. Serão feitos estudos de citotoxicidade dos compostos sintetizados, para estudar o seu efeito antitumoral, e ainda testes para avaliar a sua atividade antioxidante, uma vez que a formação de espécies reativas de oxigénio, inflamação crónica e o desenvolvimento de cancro, estão muitas vezes associados. Com base nestes estudos estabelecer-se-ão importantes relações estrutura-atividade biológica que ajudarão a perceber quais os requisitos estruturais mais importantes para a atividade destes compostos.

keywords

Cancer, pyrazoles, ruthenium complexes, antitumoral, antioxidant, anti-inflammation.

abstract

Cancer is the second main cause of death in Portugal, after cardiovascular diseases. Chemotherapy is still the most used and effective treatment, however the window in which the dose is still safe and efficient is small and consequently it can be toxic to patient's body. For that reason, the design and discovery of non-traditional antitumoral agents that are both efficient and safe is a key research issue, where pyrazoles and ruthenium (II) complexes have an important role. Several pyrazole-derived compounds have already demonstrated great antitumoral activity by inhibiting kinase enzymes such as aurora kinases and cyclin-dependent kinases, by inducing apoptosis and also by being cytotoxic to several cancer cell lines. Ruthenium complexes contribute to the antitumoral action by having redox properties and by being able to incorporate labile ligands that create, **in vivo**, active bonding sites for biomolecules.

The present work aims the synthesis of new pyrazole derivatives, following by their glycosylation and incorporation into ruthenium(II) complexes. Cytotoxicity studies will be carried out to evaluate their antitumoral effect. In addition, antioxidant activities will be studied since reactive oxygen species, chronic inflammation and cancer development are often connected. Finally, important structure-activity relationships will be established, based on the results of the biological tests, highlighting the key structural requirements needed for the activity of these compounds.

Index

List of Abbreviations

(9[aneS$_3$])	trithiacyclonane
ABTS	2,2'-azino-bis(3-ethylbenzothiazoline-6-sulphonic acid)
AGS	Human stomach gastric adenocarcinoma
ATP	adenosine triphosphate
ADP	adenosine diphosphate
BPH	benign prostate hyperplasia
CI	chronic inflammation
CDK	cyclin dependent kinase
COX	cyclooxygenase
d	duplet
dd	double duplet
DMSO	dimethylsulfoxide
DMSO-d_6	deuterated dimethylsulfoxide
DNA	deoxyribonucleic acid
DPPH	2,2-diphenyl-1-picrylhydrazyl
ERK	extracellular signal-regulated kinase
FBS	fetal bovine serum
FGF	fibroblast growth factor
GLUT	glucose transporters
HMBC	heteronuclear multiple bond coherence
HSQC	heteronuclear single quantum coherence
IC$_{50}$	half maximal inhibitory concentration
KP1019	[*trans*-RuCl$_4$(1*H*-indazole)$_2$]-imidazole
LC$_{50}$	half maximal lethal concentration
LOX	lipoxygenase
MAPK	mitogen activated protein kinase
MEK	mitogen-activated protein kinase
MRC-5	human healthy lung fibroblasts
MTS	(3-(4,5-dimethylthiazol-2-yl)-5-(3-carboxymethoxyphenyl)-2-(4-sulfophenyl)-2H-tetrazolium)
MTT	3-(4,5-dimethylthiazol-2-yl)-2,5-diphenyltetrazolium bromide
NAMI-A	[*trans*-RuCl$_4$(1*H*-indazole)(DMSO)]-imidazole
NCI	National Cancer Institute
NMR	nuclear magnetic resonance spectroscopy
NO	nitric oxide

NOESY	nuclear overhauser effect spectroscopy
PGs	prostaglandins
ppm	parts per million
PSA	prostate specific antigen
PTA	1,3,5-triaza-7-phosphatricyclo-[3.3.1.1] decanephosphine
phpz	*(E)*-3(5)-(2-hydroxyphenyl)-5(3)-arylstyryl-1*H*-pyrazoles
RAF	rapidly accelerated fibrosarcoma
ROS	reactive oxygen species
TGF	tumor growth factor
THF	tetrahydrofuran
TLC	thin layer chromatography
VGF	vascular endothelial growth factor

1. Introduction

1.1.   Scope and objectives

Cancer is the second main cause of death in Portugal after cardiovascular diseases [1] and a major health problem worldwide.

Chemotherapy is a most significant treatment strategy among the various treatment modalities available for cancer management [2]. However, the window in which the dose is still safe and efficient is small and, not rarely, toxicity problems occur in normal tissues of the body [2]. The development of cellular drug resistance is also observed [2]. For that reason, the design and discovery of non-traditional antitumoral agents that are both efficient and safe is becoming a priority in modern medicine. In the last two decades, many scientists have devoted efforts to the study of pyrazole-derivatives due to their diverse therapeutic potentials such as antileukemic [3][4] and antitumoral activities [2], by inhibiting different enzymes that are important in cell division [2].

The present work aims at developing new pyrazole-based cytotoxic compounds for cancer management, and at establishing their structure-activity relationships concerning the biological activity as cytotoxic, anti-inflammatory and antioxidant agents. In some instances the compounds will bear an α-D-Glucose substituent, aiming at selectivity. Indeed, the higher uptake of glucose by cancer cells is a well-known target for design of new antitumoral drugs [5]. In other instances, the pyrazole compounds will be coordinated to a ruthenium(II) complex, also aiming at higher cytotoxic effect as already revealed in previous studies [6]. The cytotoxicity of the compounds will be tested against the human stomach gastric adenocarcinoma (AGS) and the human healthy lung fibroblasts (MRC-5) cell lines in order to evaluate the selectivity of action for tumor cells.

Evaluation of the antioxidant properties of the new compounds is also one of our goals because there is some evidence that reactive oxygen species present in chronic inflammation may be related to the development of tumors in several organs, including those in the prostate gland and the stomach. We believe that the family of compounds

under study, for its close structural similarities to known NSAIDS‡ such as phenazone (*Antipyrin*), aminophenazone (practically not used nowadays due to risk of causing agranulocytosis) and metamizole (*Novalgin*), has the potential to offer a synergic activity, combining antitumoral and anti-inflammatory properties for a dual therapeutic effect on cancer patients.

1.1. Cancer update overview

1.1.1.   Carcinogenesis

Cancer is defined as a malignant growth caused by the uncontrolled proliferation of its constituent cells (Figure 1.1). Abnormal cell replication, as in all types of cancers, it is caused by deregulation of the cell division mechanisms. Albeit the exact cause is not easy to pinpoint, the main factors leading to this type of abnormal growth are mutations in the patients' DNA that turn on the oncogenes (responsible for supporting cell growth and vitality) or turn off tumor suppressor genes (responsible for slowing down replication, repairing DNA and starting apoptosis when DNA repair fails) [9].
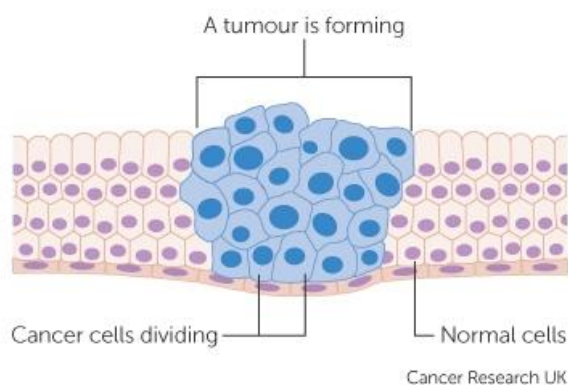
Figure 1.1 - Malignant growth caused by uncontrolled proliferation of its constituent cells originating a tumor.

---

‡ NSAIDS stands for non-steroid anti-inflammatory drugs

1.1.2. Cancer glucose uptake

Malignant cells are known for their accelerated metabolism, including higher glucose uptake [8]. Several studies were made in order to understand the exact mechanism responsible for this higher glucose uptake. One example dates back to 1990, when *Taizo Yamamoto* and his co-workers evaluated the occurrence of over-expression of facilitative glucose transporters (GLUTs) [5]. For that, they studied by RNA blotting analysis the expression of GLUTs in human cancer tissues of the digestive system and came to realize that the amounts of GLUT 1, 2 and 3 were elevated in most cancer tissues [5].

The increase of GLUTs levels in cancer cell lines encourage us to believe that the introduction of a glucose monomer in our own pyrazoles, can possible increase their cytotoxicity selectivity for cancer cell lines and perhaps exceed the main problem of common chemotherapy.

1.1.3. Cancer and chronic inflammation

Since the 19th century, when Rudolf Virchow observed the presence of leukocytes between tumors, scientists have believed that inflammation and cancer are interconnected [9]. However, only in the last decade was collected clear evidence that inflammation plays an important role in tumorigenesis [9] and that several types of cancers can arise from sites of infection, chronic irritation and inflammation [10]. Although direct causal relationship between inflammation and some cancers is not yet proven, statistics show that only 10% of all cancers are caused by germline mutations while 90% are caused by somatic mutations and environmental factors, including chronic infection (CI) microenvironments, which cause 20% of all cancers [9]. In fact, recent studies demonstrated that both cancer and CI share signaling molecules such as selectins, chemokines, and receptors for invasion, migration and metastasis [10]. Besides, CI can lead to carcinogenesis due to constant production of reactive oxygen species (ROS) and nitrogen radicals (such as nitric oxid, NO) [11]. These species damage the DNA and generate permanent genomic alterations [12] that may hamper the balance between cell proliferation and cell death [12]. Furthermore, ROS and nitrogen radicals can also damage cells by peroxidation of membrane lipids and oxidation of protein sulfhydryl group, allowing us to conclude that inflammation acts as an initiator of carcinogenesis not only

via genotoxic effects, but also *via* cytotoxic effects [11]. Even though ROS and nitrogen radicals have a short lifetime, they may still be able to live enough to diffuse through the extracellular matrix, enter the epithelial cells and damage DNA. Alternatively, cytokines such as TNF-α produced by immune cells, can stimulate ROS accumulation in neighboring epithelial cells [9].
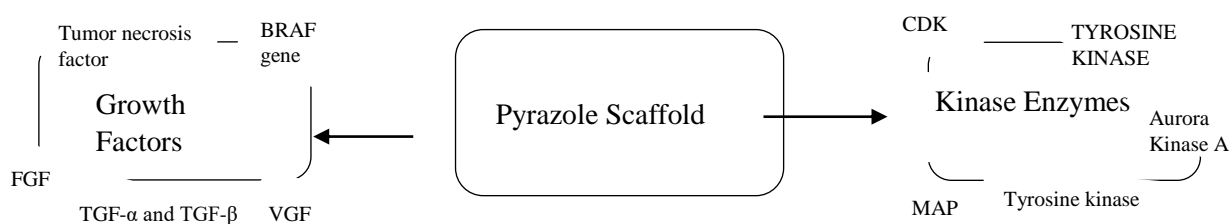
The connection between CI and prostate cancer is one example already documented. In fact, in 2006, *Gregory T. MacLennan* and co-workers [12] demonstrated the influence of CI in premalignant and malignant changes in prostatic epithelium, including prostate adenocarcinoma, by evaluating a group of 177 patients over 45 years old who presented high PSA levels or abnormal finding digital rectal examination. Their studies revealed that 20% of the patients that demonstrated CI in the first biopsy were subsequently diagnosed with adenocarcinoma during the next 5 years, while only 6% of patients with no previous CI revealed this disease during the same period of time. Furthermore, *Gregory T. MacLennan* also found higher levels of PSA in patients with prostatic inflammation compared with non-inflammated prostate revealing that CI has a significant contribution in the increase of serum PSA (Table 1.1). For that reason, we believe that the use of non-steroid anti-inflammatory drugs such as pyrazole derivatives could be a possible way to treat cancer by combining both antitumoral and anti-inflammatory activities.

Table 1.1 - Inflammation grade and serum PSA ("The influence of chronic inflammation in prostatic carcinogenesis: a 5-year follow up study", *J. Urol.*, **2006;** *vol. 176*, no. 3, pp. 1012–1016).

Inflammation grade	No. Patients	Mean ± SEM	Median (range)	p value vs no inflammation
None	31	5.91 ± 0.28	5.8 (4.1 – 11.9)	–
Mild	33	6.05 ± 0.25	5.6 (3.9 – 9.5)	0.546
Moderate	27	9.19 ± 0.25	8.8 (5.7 – 17.5)	0.0001
Severe	26	18.7 ± 1.59	16.5 (7.0 – 39.1)	0.0001

1.2. Pyrazoles in cancer

The pyrazole scaffold is extensively used in the design of new anti-cancer agents due to its highly versatile drug-like template [13]. Several pyrazole derivatives were already demonstrated to inhibit the active site of family of kinase enzymes involved in cell proliferation. Some examples are the aurora kinase, a cyclin dependent kinase (CDK), responsible for controlling chromatid segregation, the tyrosine kinase, responsible for the regulation of gene transduction cascade and the mitogen activated protein kinase (MAPK), responsible for directing cellular responses to a diverse array of stimuli [14]. Also, pyrazoles demonstrated to act at various growth factors such as the vascular endothelial growth factor (VGF), the fibroblast growth factor (FGF), the tumor necrosis factor, the tumor growth factor (TGF-α and TGF-β) and also the BRAF gene [14], as illustrated in figure 1.2.

Tumor necrosis factor — BRAF gene

Growth Factors

FGF

TGF-α and TGF-β   VGF

Pyrazole Scaffold

CDK _____ TYROSINE KINASE

Kinase Enzymes

MAP   Tyrosine kinase

Aurora Kinase A

Figure 1.2 – Representation of the possible targets for pyrazole scaffold.

Uncontrolled cell proliferation is a hallmark of cancers where kinase enzymes and tumor growth promoting oncogenes and transcription factors have an important role by progressing cancer at a faster pace [14].

1.2.1. Pyrazoles in cell proliferation
1.2.1.1. Pyrazoles as kinase enzymes inhibitors for CDK and aurora kinases inhibition

CDK are cyclin-dependent tyrosine kinases that play an important role in the control of the eukaryotic cell cycle progression [15], thus being a very good target for reseting the

cell cycle in cancer therapy [16]. A few pyrazoles with inhibitory action on kinase enzymes involved in cell proliferation, such as CDK, were already described by *Ronghui Lin* and coworkers in 2007 [17]. For example, the 3-(1*H*-benzimidazol-2-yl)-5-isoquinolin-4-ylpyrazolo[1,2-b]pyridine analogues were found to be CDK inhibitors and anti-proliferative agents, speccially for the analogue **1** (figure 1.3) [18]. Nevertheless, several properties of these compounds such as the aqueous solubility and their oral bioavailability should be improved [15], leading to proposals for structural modifications. Given that the pyrazole, imidazole and pyridinyl or isoquinoyl groups were demonstrated to have crucial CDK inhibitory activity [17], *Ronghui Lin* and co-workers proposed the use of a (*E*)-4-vinyl-pyrazole moiety to replace the bicyclic pyrazolopyridine core, the replacement of benzimidazole by an imidazole [15] and the evaluation of the corresponding activity.


2a: R^1 =H, R^2 = H, R^3 = H, R^4 = OMe ; **2b**: R^1 = H, R^2 = H, R^3 = Me, R^4 = OMe,; **2c**: R^1 = H, R^2 = -CH=CH; R^3 = -CH=CH-, R^4 = OMe; **2d**: R^1 = H, R^2 = CN, R^3 = H, R^4 = OMe ; **2e**: R^1 = **H,** R^2 = OMe, R^3 = H, R^4 = OMe; **2f**: R^1 = H, R^2 = CO$_2$Me, R^3 = H, R^4 = OMe; **2g**: R^1 = H, R^2 = CONHEt, R^3 = H; R^4 = OMe; **2h**: R^1 = H, R^2= CH^{2}NHEt, R^3 =H, R^4 =OMe; **2i**: R^1 =H, R^2 = H, R^3 = H, R^4 = 1,4-dimethylpiperazine

3a: R^1 = H, R^2=H, R^3 =H, R^4 =CF$_3$ **3b:** R^1 = H, R^2 = H, R^3 = H, R^4 = CN
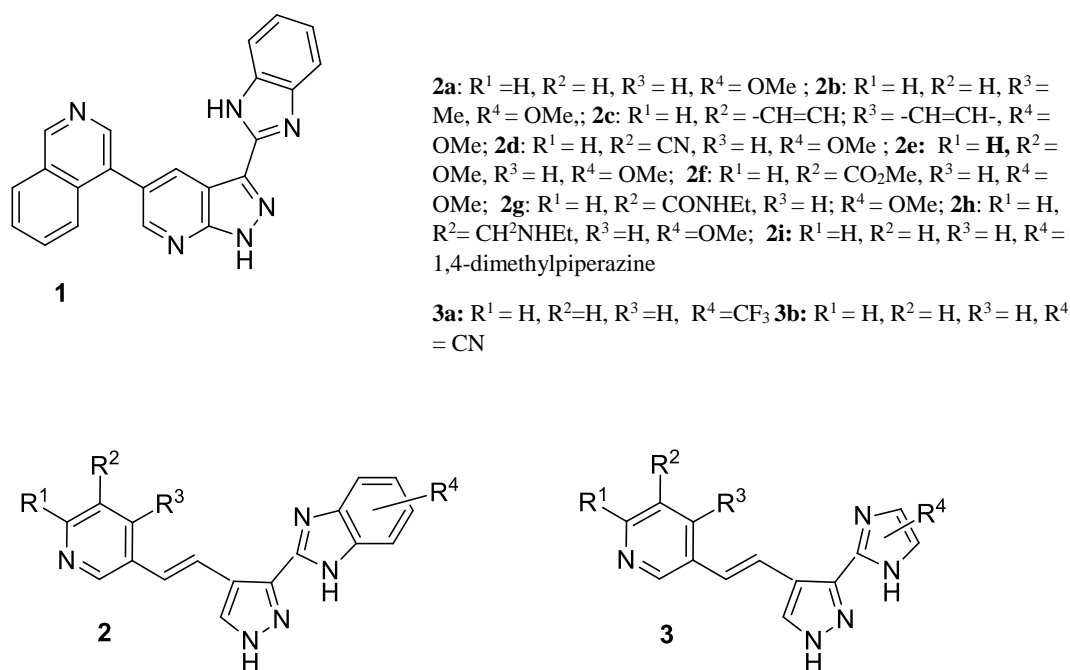
Figure 1.3 - General structure of 3-(1*H*-benzimidazol-2-yl)-5-isoquinolin- 4-ylpyrazolo[1,2-b]pyridine analogue **(1)** and 3-(benzimidazol-2-yl)-4-[2-(pyridin-3-yl)vinyl]-1*H*-pyrazoles **(2)** and 3-(imidazol-2-yl)-4-[2-(pyridin-3-yl)- vinyl]-1*H*-pyrazoles **(3).**

The derivatives were tested against different kinases aiming at determining their selectivity [15]. The results showed that the the new derivatives proved to be active *in*

vitro as anti-proliferative agents in various human tumor cell lines, such as HeLa (cervical carcinoma), HCT116 (colon carcinoma), and A375 (melanoma) and selective for CDK1, with a very good IC_{50} inhibition between 0.0046 and 0.89 μM [15]. Exceptions were observed for two derivatives (**3a**: $R^1 = R^2 = R^3 = H$; $R^4 = CF_3$ and **3b**: $R_1 = R_2 = R_3 = H$; $R_4 = CN$) that showed significantly less potent anti-proliferative activity than the other analogues [15]. However, these compounds showed slightly lower potencies when compared with the parent 3-benzimidazol-2-yl pyrazolo[3,4-*b*]pyridine series (**1**) [15], suggesting that the bicyclic pyrazolopyridine core may also be relevant for CDK1 inhibition.

Aurora kinases, another group of kinases known to be involved in multiple mitotic events (regulation of spindle assembly checkpoint pathway, function of centrosomes and cytoskeleton and cytokinesis) [19], are also a potential target for cancer therapy since its aberrant expression is typical of cancer. In fact, in 2006, *Daniele Fancelli* and coworkers discovered aurora kinase inhibition by 5-R-substituted-(phenylacetyl)pyrrolopyrazoles (**4**) (Figure 1.4). One of these derivatives, **4a** was submitted for clinical studies [20] and found to be a potent, ATP-competitive inhibitor of aurora-A kinase, with an apparent K_i value of 2.5 ± 0.3 nM [20]. *In vivo*, **4a** was effective against a range of tumor models at doses between 7.5 mg/kg and 30 mg/kg. Using the highest dose led to tumor regression and, in two cases out of eight, total remission [20].
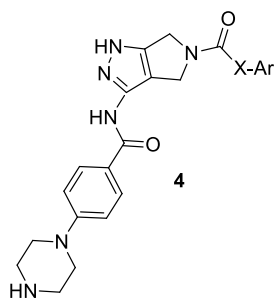
Figure 1.4. - Structure of 5-R-substituted-(phenylacetyl)pyrrolopyrazoles.
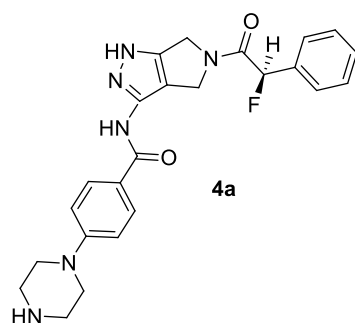
Figure 1.5 - Structure of 5-R-substituted-(phenylacetyl)pyrrolopyrazole derivative that was submitted for clinical studies.

1.2.1.2. Pyrazoles as growth and transcription factors inhibitors: BRAF and TGF inhibition

Several tumor growth promoting oncogenes and transcription factors *e.g.* TGF, FGF, B -RAF, Net, Elk-3 are suitable targets for cancer therapy. Typically, the drug inhibits the phosphorylation step of these factors, blocking signal transduction [14].

The Ras–RAF–MEK–ERK signaling pathway (Figure 1.6) is known to function a way to transduce signals from cell surface receptors to the nucleus and to give rise to the expression of genes that regulate cell growth, survival and differentiation [21]. Its activation requires binding of extracellular molecular effectors to the membrane receptor. One main class of RAS effectors is the RAF family, a group of cytoplasmic serine/ threonine protein kinases including B-RAF, the one with the strongest biochemical potential [21]. The activation of RAS by B-RAF can activate MEKs and consequently ERKs, responsible for phosphorylation of some transcription factors [21]. Several mutations in B-RAF have been detected in some types of cancers, however the single base substitution at nucleotide 600 is the most common one and it is characterized by a substitution of a valine by a glutamic acid that consequently forms an independent RAS B-RAF protein, resulting in uncontrolled proliferation [21].

Some small chemical structures containing the pyrazole scaffold have been already described as BRAF^{V600E} inhibitors and anti-cancer agents [22]. In fact, in 2012, *Qing- Shan Li*,, encouraged by previous positive results, has designed more than 300 diverse novel potential BRAF^{V600E} inhibitors for anti-melanoma agents based on the pyrazole

8

skeleton [22]. Of these ~300 different analogues, six where selected for protein-kinase inhibitory activity studies, after a previous screening. Two candidates, **5** and **6** (Figure 1.7) were chosen for further study due to their very low values of IC_{50} againt $BRAF^{V600E}$ [22]. [(5-(4-(benzyloxy)phenyl)-3-(4-methoxyphenyl)-4,5-dihydro-1*H*-pyrazol-1-yl)(5-bromo-2-hydroxyphenyl)methanone (**5**) was shown to form extensive hydrophobic interactions with the Val 471, Ala 481, Lys 483, Leu 514, Ile 527, Thr 529, Phe 583 and Asp 594 residues of the ATP-binding pocket of BRAF kinase[22]. These positive results suggest that the 3,5-diarylpyrazoline skeleton of **5** and **6** could serve as a promising scaffold for developing new kinase inhibitors of V600E mutant BRAF [22]. However, in order to understand the inhibitory action of this pharmacophore and optimize the structure for rationally, *Shan Li.* also used **5** and **6** as models for the design and synthesis of new derivatives maintaining the methoxyl and phenolic hydroxyl groups because they are beneficial for its binding affinity with mutant BRAF[21]. Once again, these derivatives inhibited $BRAF^{V600E}$, suggesting that the pyrazole scaffold (in particular, 3,5-diarylpyrazoline) is indeed useful as a novel scaffold for the further development of more potent and selective $BRAF^{V600E}$ inhibitors and as therapeutic agent on mutant BRAF-dependent tumors [22].
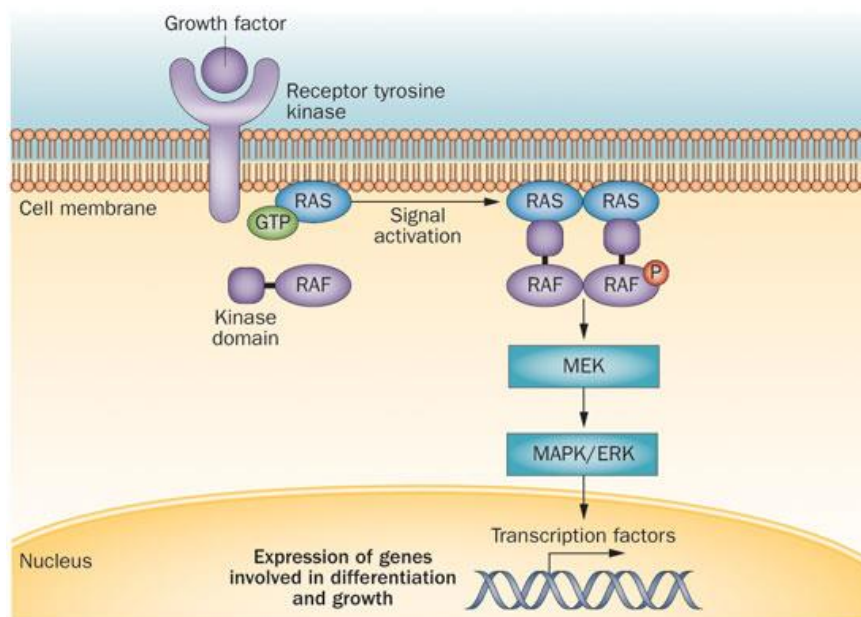
Figure 1.6- Scheme showing the activation of the RAS–RAF–MEK–ERK signaling pathway under normal conditions [23]. The GTPase RAS is recruited to the plasma membrane and consequently activated. The

RAF kinase domain binds to RAS, activating the kinase cascade and producing the signal transduction that results in the expression of genes involved in differentiation and growth.
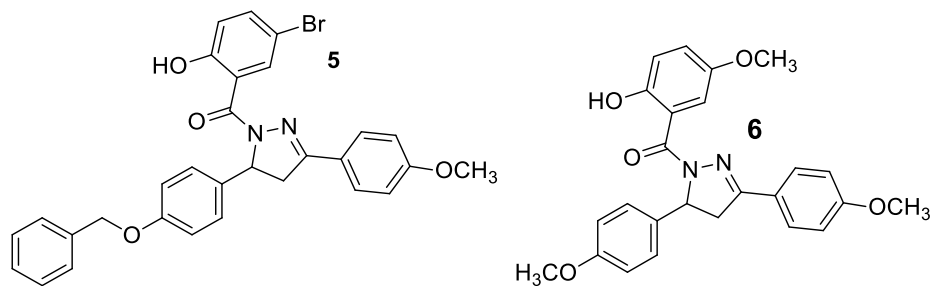

Figure 1.7- Structure of **5** and **6**.

1.2.2. Pyrazoles in the apoptotic pathway: p53-mediated and TRAIL-mediated apoptosis effect

A few pyrazole derivatives were shown to restore the apoptotic pathway that leads to cell death [13]. In fact, 1*H*-pyrazol-4-ylcarbonylthiourea derivatives were described with high-apoptotic effect, namely *N*-[(1-methyl-1*H*-pyrazol-4-yl)carbonyl]-N'-(R-phenyl)-thiourea compounds (Figure 1.8) [13] **(7)**, designed using tenovin-1 **(8)** and AW00178 **(9)** (Figure 1.9) as patterns due to their action in p53-mediated [24] and TRAIL-mediated apoptosis [25], respectively.
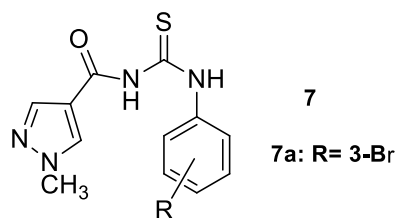

Figure 1.8 - General structure of *N*-[(1-methyl-1*H*-pyrazol-4-yl)carbonyl]-N'-(R-phenyl)thiourea derivatives (**7**).
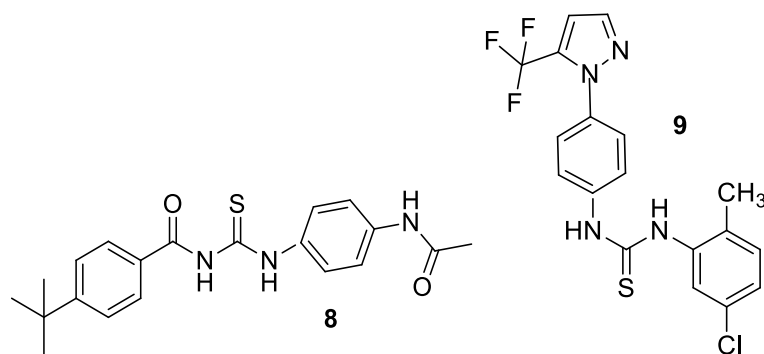
Figure 1.9 - Structure of tenovin-1 (*left*) and AW00178 (*right*).

The activity of compounds on cell viability was evaluated using the MTS assay and cellular apoptosis was analyzed by flow cytometry. Human carcinoma cell lines such as THP-1 (monocytic leukemia), HCT-8 (colorectal adenocarcinoma) and HEp-2 (cervix carcinoma) were employed [13]. Cell viability results showed that *N*-[(1-methyl-1*H*-pyrazol-4-yl)carbonyl]-*N'*-(3-bromophenyl)thiourea **(7a)** was the most effective in suppressing cell growth, decreasing viability from 100% to 32±8.2 (%) on THP-1 and 78.2±3.3 (%) on HCT-8 after 24 h of 50 µg/mL exposure [13]. All compounds demonstrated small effect on HEp-2 cells [13]. The results for both late and early apoptosis, together with necrosis, demonstrated that **7a** was again the most effective among all derivatives. It was shown to increase TRAIL-R2 and TRAIL-R1 expression, both tumor necrosis factor receptors that are activated by tumor necrosis factor-related apoptosis-inducing ligand (TRAIL) and activate caspase 3 [13] (Figure 1.10). It was also demonstrated to reduce two anti-apoptotic proteins with tumorigenic activity, Hsp70 and Hsp27 (Figure 1.11), and to increase the phosphorylation of p53, being thus able to activate apoptosis via p53 pathway [13]. For that reason, **7a** could be a promising anti-cancer agent to be developed in animal model.

TRAIL

Cell
membrane   TRAIL-R2   TRAIL-R1

FADD

Pre-Caspase 8

Caspase 8

Pre-Caspase 3

Caspase 3
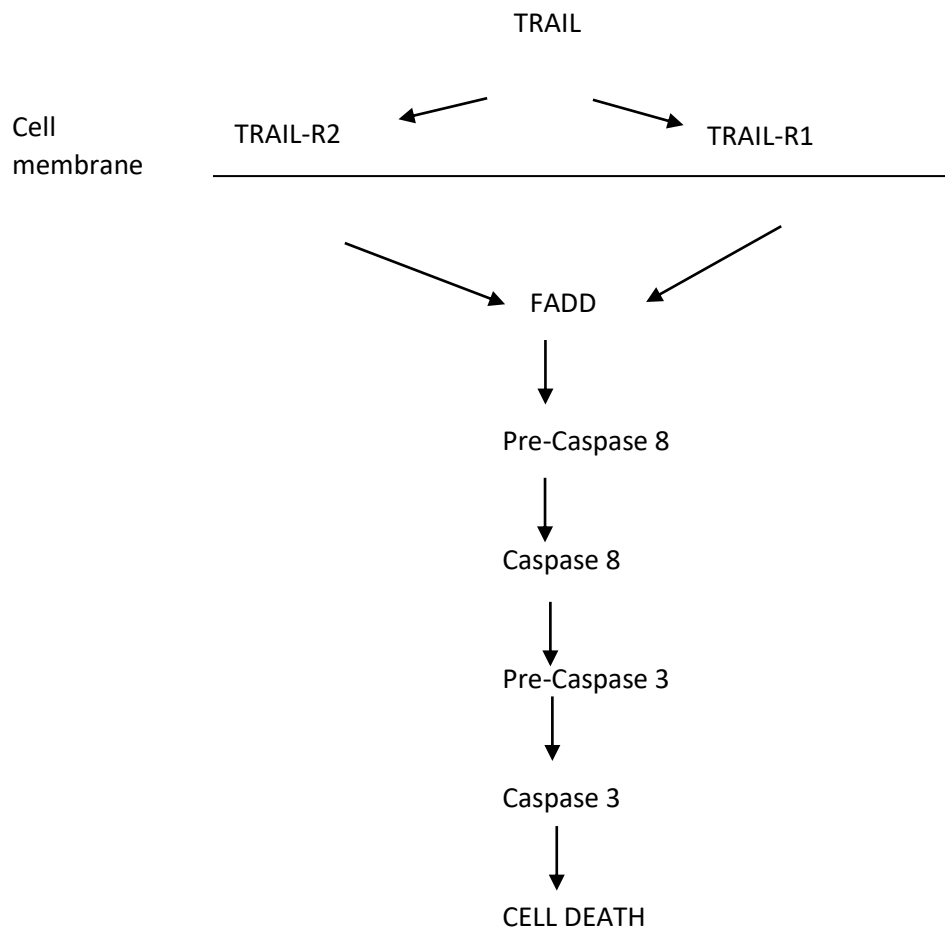
CELL DEATH

Figure 1.10 – Representation of TRAIL-mediated apoptosis mechanism. TRAIL are recognized by TRAIL-1 and TRAIL-2 receptors that consequently initiate caspase cascade that leads to cell death. The derivative **4a** increases this mechanism by overexpressing TRAIL-1 and TRAIL-2 [13].
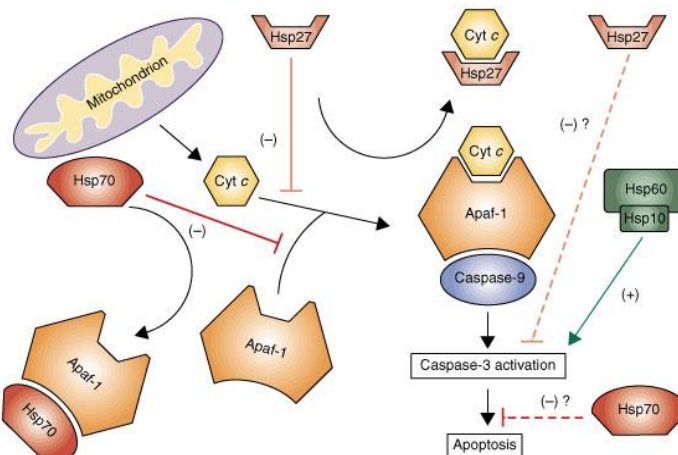
1.2.3.   Pyrazoles and protein folding: inhibition of Hsp90
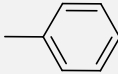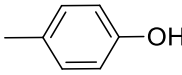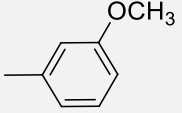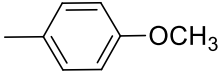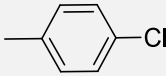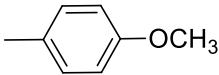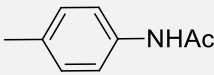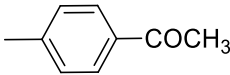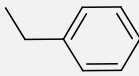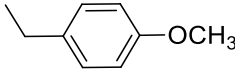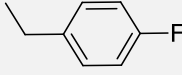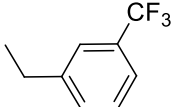
The chaperone protein Hsp90 (heat shock protein 90) is responsible for maintaining conformation and stability of proteins involved in signal transduction, cell cycle regulation and apoptosis; it can also be a target for pyrazole compounds. The 3(5)-(2-hydroxyphenyl)pyrazole family, in particular, has demonstrated strong inhibition on this enzyme. It is known that inhibition of the active site of Hsp90 in cancer cells can cause apoptosis and degradation of some proteins involved in cell growth. For that reason, targeting for Hsp90 is a promising strategy in cancer therapy.

Paul A. Brough and coworkers studied the inhibition effect of new 3-(5-chloro-2,4-dihydroxyphenyl)pyrazole-4-carboxamides for Hsp90 using VER-49009, a small inhibitor, as a template [27] (Figure 1.12) in order to understand how structural changes can affect selectivity against Hsp90 the consequent inhibition cancer cell growth. All derivatives were tested for the ATP binding site using fluorescence polarization. The results for ATP binding site and cell growth inhibition obtained on this study were all in the micromolar range, as presented in table 1.2.
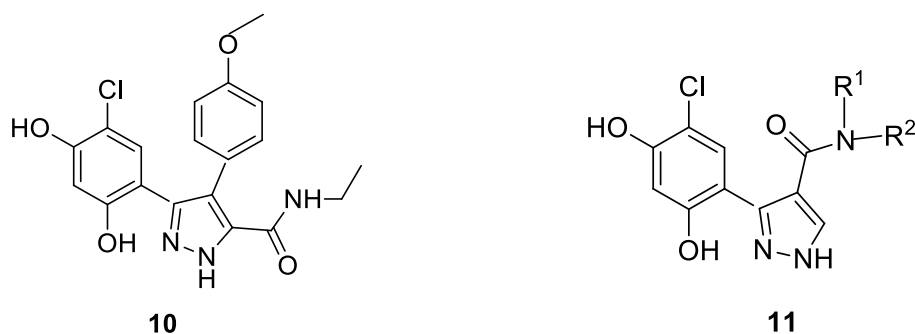
Figure 1.12 - General formula of VER-49009 (**10**) and new 3-(5-chloro-2,4-dihydroxyphenyl)-pyrazole-4-carboxamides (**11**).

Table 1.2 - Mean results obtained for Hsp90 binding site (given by fluorescence polarization) and for *in vitro* growth inhibition displayed by new 3-(5-chloro-2,4-dihydroxyphenyl)pyrazole-4-carboxamides analogues [27].

Compound	R_1	R_2	FP Enzyme IC_{50}, µM	Cell growth inhibition IC_{50}, µM
11a	H	phenyl	7.1	nd
11b	H	4-OH-phenyl	14.7	>80
11c	H	2-OCH_3-phenyl	11.7	>80
11d	H	4-OCH_3-phenyl	6.0	>80
11e	H	4-Cl-phenyl	6.9	>80
11f	CH_3	4-OCH_3-phenyl	>50	nd
11g	H	4-NHAc-phenyl	31.5	59.7
11h	H	4-$COCH_3$-phenyl	0.258	11.6
11i	H	benzyl	12.8	>80
11j	H	4-OCH_3-benzyl	6.0	60.7
11k	H	4-F-benzyl	5.35	>80
11l	H	3-CF_3-benzyl	5.40	45

11m	H		0.461	>80

The most effective analogue was the one with an acetyl group at the *para* position of the phenyl ring (**11h**), with $IC_{50} = 0.285\mu M$ [27]. The reason for this good activity may be due to the oxygen of the acetyl group that can establish hydrogen bonds with the Phe138 of Hsp90, in the same way as the analogue with a sulfoxide group at the *para* position of the phenyl ring. Besides, the analogue **11h** presented a low micromolar range for *in vitro* cell growth inhibition (~ 11.6 µM) possibly indicating a good cell penetration.

The analogue **11m** demonstrated to be a great inhibitor for Hsp90 presenting an IC_{50} micromolar range of 0.461µM. However when testing **11m** for *in vitro* cell growth, it demonstrated a high IC_{50} micromolar range of > 80 µM. These results can be explained by a possible poor cell penetration that hinders the entrance of such compound into the cell and consequently needing higher concentrations to be available inside the cell and to inhibit Hsp90 [27].

These results show the importance of Phe138 on the active site of Hsp90, since it is the residue that binds to ADP by hydrogen bonds [27]. Furthermore, we can postulate that 3-(5-chloro-2,4-dihydroxyphenyl)pyrazole-4-carboxamides are potential Hsp90 inhibitors, where the existence of a R^2 substituent capable of establishing hydrogen bonds to Phe138 increases their binding affinity [27].

1.2.4.   Cytostatic and cytotoxic effect against tumor cell lines

We know that pyrazole derivatives can act as possible antitumor agents by acting in different mechanisms such as apoptosis, cell growth and others. However, the exact mechanism of the chemotherapeutic action of some of these derivatives is still unknown. Such is the case of several new 1-(4-chlorophenyl)-4-hydroxy-1*H*-pyrazole-3-carboxylic acid hydrazide derivatives showing the general formula (**12**) that exhibited potential antitumor activity, often associated with high or moderate selectivity for certain human tumor cell lines [2]. Three of these compounds were selected, together with 1,3,4-oxadiazole and 1,2,4-triazole moieties, by the NCI's biological committee for subsequent confirmatory screening procedures in order to understand their mechanism of action [2]. Based on these results *Sherif A. F. Rostom* and coworkers were inspired to explore

additional modifications at position 3 of the pyrazole scaffold while maintaining the 1-(4-chlorophenyl)-4-hydroxy-1*H*-pyrazole template [2]. This study was mainly focused on the effect of using various polysubstituted pyrazole counterparts linked by a carbonyl bridge **(13)** or nitrogenous heterocycles linked by and amide bridge **(14)** in order to achieve better hydrogen-bond centers or even to achieve possible new biological activities [2].
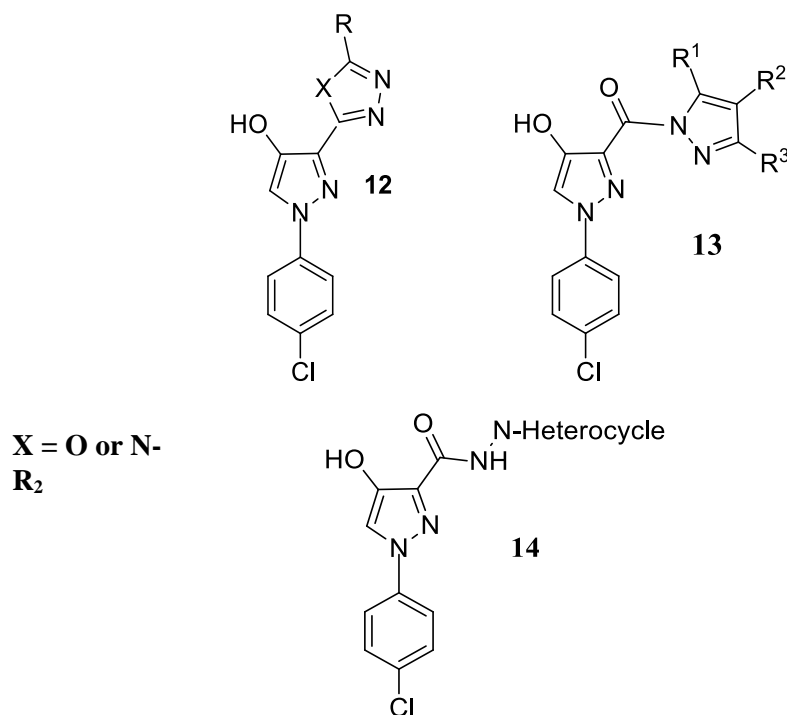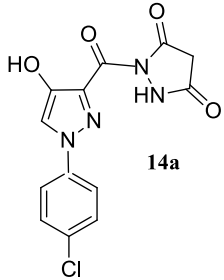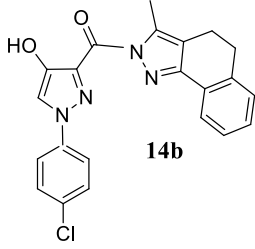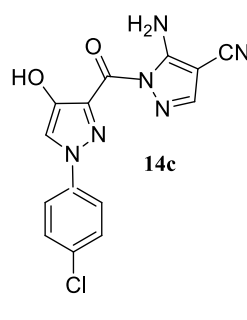
Figure 1.13 - General formula of new 1-(4-chlorophenyl)-4-hydroxy-1H-pyrazole-3-carboxylic acid hydrazide derivatives (**12**) and new 3-polysubstituted 1-(4-chlorophenyl)-4-hydroxy-1H-pyrazoles (**13**) and **14**.

Out of the newly **14** polysubstituted 1-(4-chorophenyl)-4-hydroxy-1*H*-pyrazoles   ten were selected by the National Cancer Institute (NCI) for *in vitro* disease-oriented human cells screening assays to be evaluated for their *in vitro* antitumor activity against leukemia, non-small cell lung, colon, CNS, melanoma, ovarian, renal, prostate and breast cancer cell lines [2]. Within these ten, six were found to be the most effective, but only three of them were selected by NCI's committee for follow-up studies on their mechanism of action, as illustrated on table 1.3. These choice of the NCI's committee was based on

their median growth inhibitory concentrations (IG_{50}), median total growth concentrations (TGI) and lethal concentrations 50 (LC_{50}) [2]. The results are presented in the Table 1.3.

Table 1.3 - Structures of the three new polysubstituted 1-(4-chorophenyl)-4-hydroxy-1*H*-pyrazoles selected by NCI's committee and their respective GI_{50}, TGI and LC_{50} for each type of the cell lines selected for the biological tests by *Sherif A. F. Rostom* and coworkers [2]

Structure	GI_{50} (µM)[a]	TGI (µM)[b]	LC_{50}(µM)[c]	Cell lines[d]
14a	0.42	10.8	-	I
	0.51	80.3	-	II
	1.51	86.2	-	III
	0.33	87.9	-	IV
	1.60	50.1	85.2	V
	1.08	84	-	VI
	0.85	71.8	-	VII
	0.67	-	-	VIII
	0.82	79.6	-	IX
14b	0.042	10.2	90.7	I
	0.047	68.1	-	II
	0.221	86.3	-	III
	0.036	69.1	-	IV
	0.140	52.1	86.4	V
	0.115	83.6	-	VI
	0.092	67.7	-	VII
	0.044	-	-	VIII
	0.082	91.7	-	IX
	0.27	3.23	44.3	I
	0.32	10.8	69.4	II
	0.61	12.6	64.3	III
	0.32	23.1	74.7	IV
	0.46	11.9	65.0	V
	0.50	19.6	88.5	VI

	0.36	8.99	75.0	VII
	0.45	13.4	-	VIII
	0.43	14.4	64.3	IX

(a), (b) and (c) – Median values calculated according to the data obtained from NCI's in vitro disease-oriented human tumor cell screen (d) – I, Leukemia; II, non-small cell lung cancer; III, colon cancer; IV CNS cancer; V, melanoma; VI, ovarian cancer; VII renal cancer; VIII, prostate cancer; IX, breast cancer[2].

Table 1.4 - Results for panel mean-graph mid-point (MG-MID) that represents the average sensitivity of all cell lines towards the test agent

Compounds	MG-MID (IC_{50})	MG-MID (TI)	MG-MID (LC_{50})
14a	0.67	53.8	93.3
14b	0.08	30.9	93.3
14c	0.36	8.78	69.3

Looking at the previous results, we can notice that **14c** presented a remarkable cytotoxic effect for almost all cell lines, when compared to the other two derivatives, probably because the presence of the primary amine that can improve the solubility of the compound. It was also, together with **14b**, the most effective agent inhibiting cell growth and proliferation. It is important to notice that **14c** was the only compound able to inhibit and kill prostate cancer cells, the target of our present work.

All the three compounds have in common a carbonyl group linking both pyrazoles moieties, indicating that is an essential pharmacophore for potential anticancer activity, together with other functionalities that could assist in hydrogen bond formation [2].

More recent studies also revealed the anticancer potential of new pyrazoles such as imidazo[1,2-b]pyrazoles which were synthesized and screened by Sandrine Grosse and coworkers in 2014 without highlighting the exact mechanism of their action [28]. Their

work relied on the synthesis of C-2/C-6/C-7 trisubstituted; C-2/C-3/C-6 tri(hetero)arylated and C-2/C-3/C-6/C-7 tetrasubstituted imidazo [1,2-b]pyrazoles [28] and they evaluated how structure changes can influence the biological activity of these compounds. However, from all the 39 compounds synthesized, only four displayed an IC50 ≤ 10 µM against all the tested cell lines. The structures of the compounds are presented in figure 1.14.
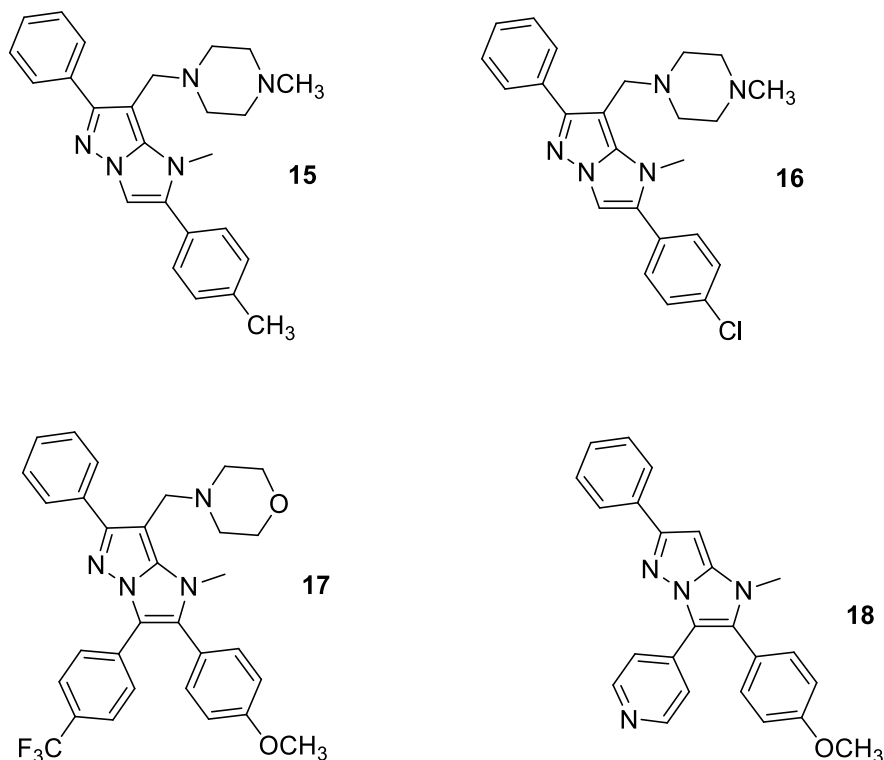
Figure 1.14 - Two *C-2/C-6/C-7 trisubstituted imidazo[1,2-b]pyrazoles* (**15** and **16**); One *C-2/C-3/C-6 tetrasubstituted imidazo[1,2-b]pyrazole* (**17**) and one *C-2/C-3/C-6/C-7 tri(hetero)arylated imidazo[1,2-b]pyrazole* (**18**); the four compounds that demonstrated to have IC$_{50}$≤ 10 µM (the concentration of the compound that reduces by 50% the global growth of a given cell line after three days of culture in presence of the compound) [28].

A careful analysis of the structures of compounds **15** and **16** allowed the researchers to conclude that the introduction of a cyclic aminomethyl group in the *C-2/C-6/C-7 trisubstituted imidazo[1,2-b]pyrazoles* appears to afford highly promising antitumoral candidates at least *in vitro* due to their IC$_{50}$ values against six cell lines of 5 and 4 µM, respectively [28]. They also concluded that from all *C-2/C-3/C-6/C-7 tri(hetero)arylated imidazo[1,2-b]pyrazoles,* compound **18** was the only one which exhibited satisfactory

results with an IC_{50} of 1.6 µM , probably due to presence of the pyridine ring that is postulated to improve penetration into the cell membrane [28]. They also concluded that the introduction of a fourth group is not beneficial when comparing to other structures of these families, except for compound **17** [28], probably because of the presence of flour known for, in special conditions, increase the affinity for target proteins, polarity, etc. These studies show that pyrazoles can provide a good scaffold for anticancer drug candidates when subject to a careful structural design. A particularly relevant structural feature is the lipophilicity, for reasons concerning permeability to cell membrane.

1.3.Pyrazoles as antioxidant
1.3.1.   Antioxidant activity

Cells are continuously generating reactive oxygen and nitrogen species and free radicals when exposed to an aerobic environment [29]. Excessive or inappropriate production of these species is commonly associated with several diseases such as atherosclerosis, arthritis, neurodegenerative disorders and even cancer [29]. As mentioned before, CI can be responsible for carcinogenesis due to the generation of such reactive species resulting in DNA damage [12]. Therefore, many authors believe that cancer incidence in an ageing population could be reversed by removing ROS or by enhancing the antioxidant defense system [29].

Pyrazole derivatives already demonstrated a lot of potential on different biological activities including anti-inflammatory and antioxidant [30]. Moreover, other heterocycles in association with pyrazoles play an important role in chemical and pharmacological fields [31], inspiring scientists to synthesize new and better heterocyclic compounds containing the pyrazole scaffold. One example is the use of dendritic antioxidants with pyrazole as the core, improving the ability to scavenge radicals and consequently protecting DNA [32].

Dendrimers are widely used in drug development due to their special affinity for DNA and membranes and also for their action on other biological activities. In 2012, *Yan-Feng Li* and coworkers, studied the improvement of the antioxidant effect of dendrimers by using pyrazoles as the core [32]. The aim of the project was to synthesize four different pyrazole derivatives maintaining a dendritic structure (**TPP, BPP, APP, CPP**) and reveal

the antioxidant effect of the N atom of pyrazole [32]. Their structures are presented on figure 1.15.

19

19a (TPP): $R^1=R^2=R^3=H$
19b (BPP): $R^1=R^3=H$; $R^2=OH$
19c (APP): $R^1=OH$; $R^2=R^3=H$
19c (CPP): $R^1=R^3=H$; $R^2=OH$
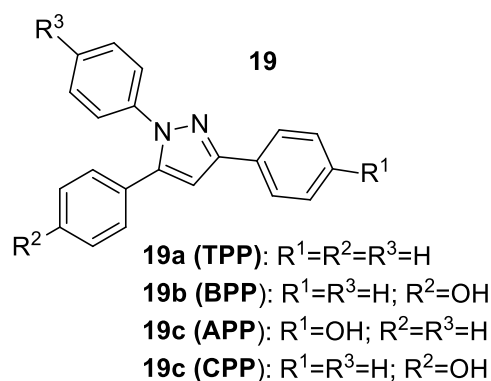
Figure 1.15 - General structure of 1,3,5-triphenyl-1H-pyrazole **(TPP)**, 4-(1,3-diphenyl-1*H*-pyrazol-5-yl)phenol **(BPP)**, 4-(1,5-diphenyl-1H-pyrazol-3-yl)phenol **(APP)** and 4-(3,5-diphenyl-1*H*-pyrazol-1-yl)phenol **(CPP)**.

The obtained compounds were tested for their antioxidant effect by using 2,2'-azino-bis(3-ethylbenzothiazoline-6-sulphonic acid) (ABTS) and 2,2-diphenyl-1-picrylhydrazyl (DPPH) assays. The results showed that all four derivatives have a similar ability to trap ABTS and DPPH, including **TPP**, the unsubstituted compound, i.e, having no hydroxyl group. Thus, *Yan-Feng Li* and coworkers were able to conclude that the pyrazole nucleus can actually act as antioxidant due to the presence of an electron pair in the nitrogen atom that traps ABTS+• and DPPH radicals by donating its electron [32]. The similar number of $ABTS^{+\cdot}$ and DPPH radicals trapped *(n)* by all four derivatives further indicated that the introduction of a phenolic hydroxyl group does not increase the ability to trap radicals [32]. However, looking at table 1.5., we can see that the number of ABTS+• and DPPH trapped by the oxidized products of the antioxidant *(n_{app})* were different between all derivatives, even for those with the same number of ABTS+• and DPPH trapped by the antioxidant primary period (*n*). These results, indicate that the total ability to trap radicals is largely derived from the oxidized products of these compounds [32].

Table 1.5 - Values for the number of ABTS+• and DPPH trapped *(n)* by the antioxidant primary period and by the oxidized products of the antioxidant *(n_app)*, provided by *Yan-Feng Li* in *2012* [32].

Free Radical	Antioxidant	n	n_{app}	$n+n_{app}$
DPPH	TTP (**19a**)	0.08±0.01	0.09±0.01	0.17±0.01
DPPH	APP (**19c**)	0.08±0.01	0.14±0.01	0.22±0.01
DPPH	BPP (**19b**)	0.07±0.01	0.06±0.01	0.13±0.01
DPPH	CPP (**19d**)	0.07±0.01	0.08±0.01	0.15±0.01
ABTS+•	TTP (**19a**)	0.25±0.01	0.22±0.01	0.47±0.01
ABTS+•	APP (**19c**)	0.28±0.01	0.12±0.01	0.40±0.01
ABTS+•	BPP (**19b**)	0.25±0.01	0.16±0.01	0.41±0.01
ABTS+•	CPP (**19d**)	0.25±0.01	0.27±0.01	0.52±0.01

Looking at the table 1.5 we can conclude that the oxidized species of **APP** and **BPP** are both the better trappers for ABTS+• and DPPH, respectively. Their trapping ability is actually not very different from those of traditional phenolic compounds. This may be due to the benzene ring in these pyrazole derivatives which does not completely form a conjugation system with the pyrazole ring and consequently the phenolic radical is not stabilized by the whole conjugation system [32].

1.3.2. Anti-inflammatory activity
1.3.2.1.   Pyrazole as COX inhibitors: COX-2 selectivity

Cyclooxygenases (COX) play an important role in inflammation by converting arachidonic acid to pro-inflammatory prostaglandins (PGs) [33], inflammatory mediators (Figure 1.16.). Several NSAIDs are used for therapeutic management of acute and chronic inflammation, pain, and fever, by inhibiting COX and consequently reducing prostaglandin production [34]. Despite of the main use of these drugs by population and the continuous research to improve their pharmacological index, NSAIDS still presents a high incidence of ulcerogenicity [35], evidencing the need for the search of new anti-inflammatory and COX-inhibiting agents.

There are two isoforms of COX (COX-I and COX-II). The COX-I is responsible for the synthesis of PGs involved in the regulation of physiological cellular activities and it is

expressed in most tissues and organs. The COX-II is mainly stimulated by various stimuli such as cytokines, mitogens, and endotoxins in inflammatory sites [35].
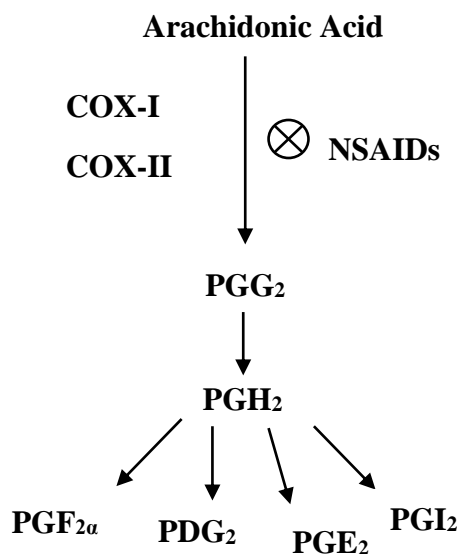
Figure. 1.16 – Representation of the conversion of arachidonic acid to prostaglandins by action of COX-I and COX-II and the action of NSAIDS by inhibiting both enzymes and consequently inhibiting the production of PGs.

Several heterocyclic compounds already demonstrated their potential to inhibit COX. Pyrazole is found in the scaffold of Celecoxib [36], a commercially available NSAIDs, inhibiting selectively COX-2 [37] and thus preventing the synthesis of pre-inflammatory prostaglandins. The other marketed structural analogues of Celecoxib (**20**), shown in figure 1.17, do not present the pyrazole ring. Note that Rofecoxib (**21**) was banned in 2004 because of cardiac toxicity, probably associated to its metabolism [36].
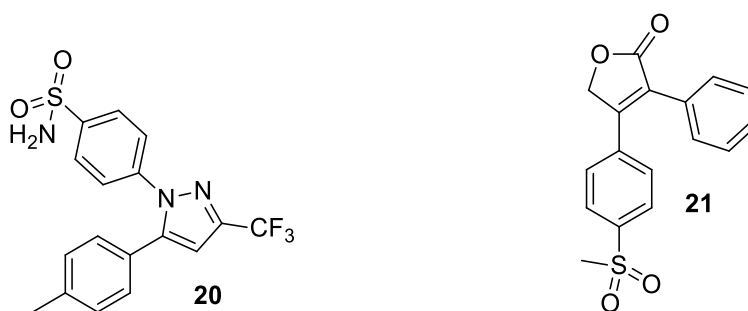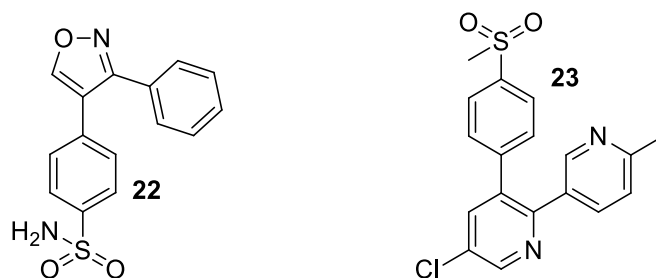
Figure 1.17 – Structure of the commercial COX-2 inhibitors including the one carrying the pyrazole scaffold, Celecoxib (**20**).

In fact, in 2011 *Magda A.-A. El*-Sayed and coworkers synthesized some new hydrazone and pyrazole derivatives and studied their COX-inhibition activity [36]. The results showed that the compounds which demonstrated the best inhibitory profiles against COX-2 were pyrazole derivatives (**23**, **24a** and **24d**) wish structure is presented in figure 1.19. The best hydrazone derivative is also illustrated on figure 1.18.

22a: R = Cl; $R^1=R^2=R^3=$H
22b: R^1 = Cl; $R^2=R^3=$R=H
22c: R^2 = Br; $R^1=R^3=$R=H
22d: R^2 = NO_2; $R^1=R^3=$R=H
22e: R^2 = OCH_3; $R^1=R^3=$R=H
22f: R=R^2=H; $R^1=R^3=CF_3$
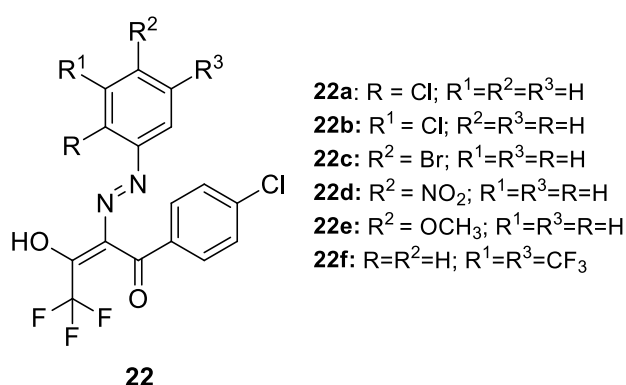
Figure 1.18 – General structure of the hydrazone derivatives with COX-2 inhibitory profile, including the non-pyrazol most active compound **22f.**

24a: n=0
24b: n= 1
24c: n= NCH_3
24d: n= NC_2H_5
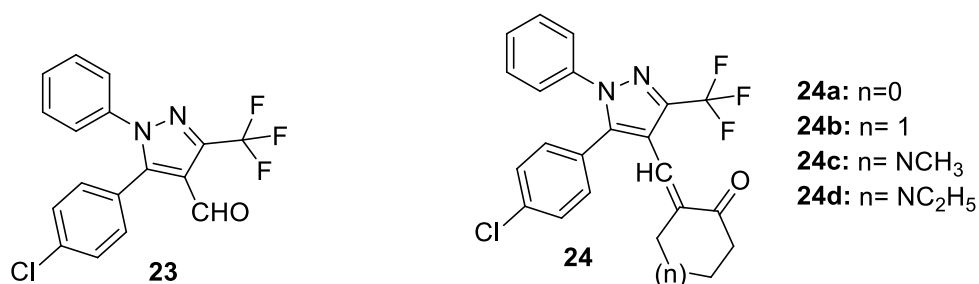
Figure 1.19 – Structure of pyrazole derivatives that showed COX-2 inhibitory activity.

Molecular docking studies were employed to help understand the mechanism of the selective action of these pyrazole derivatives on COX-2, The existence of an additional pocket in COX-2, (absent in COX-1) is very important in the design of selective COX-2 inhibitors [36]. This additional pocket may be due to the replacement of Ile523 of COX-1 by Val523, a less bulky aminoacid [36]. The molecular docking sites, in fact, showed that pyrazole derivatives, when having the appropriate substitution, can fill this second pocket and also interact with the relatively polar residues such as Gln192 and Arg513. Furthermore, compounds 1**6a** and 1**6d** were shown to have four strong hydrogen-binding sites [36].

Other studies proved once again the selectivity of pyrazole scaffold towards COX-2, such as the study reported by *S. G. Alegaon* and coworkers in 2014 [38]. In their study, a series of 1,3,4-trisubstituted pyrazole derivatives were synthesized and evaluated for their cyclooxygenase (COX-1 and COX-2) inhibitory activity. Molecular docking showed better interaction with the active site of the docked receptor COX-2 than with that of COX-1, suggesting that using the pyrazole as scaffold can actually be an interesting approach in the design of new selective COX-2 inhibitors [38].

1.3.3. Pyrazole templates as LOX inhibitors: 5-LOX and 15-LOX selectivity

1.3.3.1. 5-LOX selectivity

The mammalian lipoxygenases (LOX) belong to a family of structurally related lipid peroxidizing enzymes that have a particular role in inflammatory diseases [39] as shown on figure 1.20. Their function is to insert a molecule of oxygen into arachidonic acid at carbon 5, 12 or 15, depending on the type of the enzyme [39].

Inhibition of 5-LOX has already shown therapeutic value for the treatment of asthma, allergic rhinitis, atherosclerosis, and cancer [40]. However, only zileuton has been approved by the FDA to treat asthma in the USA, therefore the development of new effective structures against 5-LOX warrants further efforts [40].
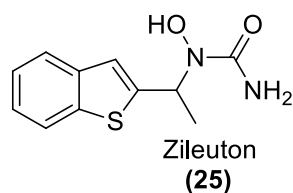
Zileuton
(25)

Figure 1.20 – Structure of zileuton, the only 5-LOX inhibitor approved by FDA to treat asthma.

In 2014, a series of 1,4-dihydrothieno[30,20:5,6]thiopyrano-[4,3-c]pyrazole-3-carboxamide derivatives were reported as potential inhibitors of 5-LOX by Jianshu Hu1 and coworkers [40].
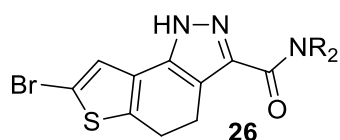
Figure 1.21 – Structure of *1, 4-dihydrothieno [30, 20:5, 6]thiopyrano-[4, 3-c]pyrazole-3-carboxamide* derivatives with potential activity against 5-LOX.

Among all the compounds tested, the derivative possessing a *4-(2-fluorophenyl)piperazinyl* substituent at position R_2, showed the most significant inhibitory effect against 5-LOX with an IC_{50} around 5.7 µM (similar to Zileuton) [40]. This result was explained using molecular docking studies.

Looking at figure 1.22, provided by *Jianshu Hu1*. and coworkers [40] we can see that the nitrogen atom of the pyrazole ring is responsible for hydrogen bonding with Thr247, thus evidencing that pyrazole scaffold is important for 5-LOX inhibition. However, as we can see in this particular study, the substituents on the pyrazole template play an important role in enzyme selectivity. For example the 4-(2-fluorophenyl)piperazinyl group of the most active derivative, is located in the site comprising Leu297, Ile556 and Leu490 of 5-LOX [40].
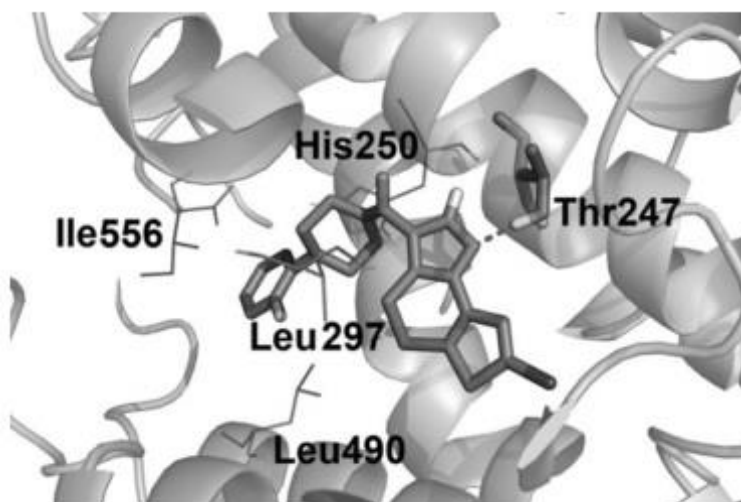
Figure 1.22 - Binding mode of the 1,4-dihydrothieno [30, 20:5, 6]thiopyrano-[4,3-*c*]pyrazole-3-carboxamide derivative with a 4-(2-fluorophenyl)piperazinyl substituent at position R_2, showing the 5-lipooxygenase substrate binding site as predicted by molecular docking.

However, this compound does not show significant inhibition against the other two types of LOX (12-LOX and 15-LOX), thus corroborating its selectivity against 5-LOX [40]. This study revealed the importance of pyrazole template regarding the inhibition of 5-LOX, but also how the whole compounds' structure is important to change the activity and the selectivity.

1.3.3.2. 5-LOX selectivity

As mentioned before, there are three types of mammalian LOX, depending where the oxygen atom is positioned in the arachidonic acid. Once again pyrazole ,proved to be a valuable scaffold as anti-inflammatory agent by inhibiting another type of human lipoxygenase (15-LOX) [39].

In 2015, *Benjamin Pelcman* and coworkers demonstrated the ability of *N*-substituted pyrazole-3-carboxamides to inhibit human 15-LOX in vitro [39].
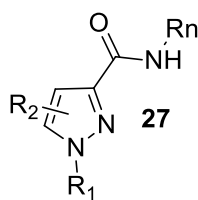
Figure 1.23 – Structure of *N-substituted pyrazole-3-carboxamides* with potential 15-LOX inhibitory activity.

1.4. Ruthenium complexes as antitumoral agents

Since the discovery of the antitumoral effect of cisplatin, metallic complexes have become a subject of discussion and interest among the scientific community.

Ruthenium complexes, in particular, present a set of properties that are useful for antitumoral action, namely the versatile ligand-exchange abilities, redox properties and octahedral geometry [41]. Ruthenium redox properties can be changed according to the type of the ligand. It is known that compounds such as glutathione and ascorbate are able to reduce ruthenium(III) to its most active biological form. Therefore, when approaching infected sites, the low pH and the high amount of glutathione keep a redox environment and ruthenium(III) is reduced to ruthenium(II) [42]. In addition to these characteristics, ruthenium also presents low toxicity [42].

1.4.1. Ruthenium(III) complexes and cancer

The most successful examples of ruthenium(III) with antitumoral activity are NAMI-A and KP1019. The NAMI-A (imidazolium [trans-RuIIICl4(DMSO)imidazole])[43] (Figure 1.24.), that was the first ruthenium complex to enter clinical trials, showed anti-metastatic action *in vitro* but poor effect on phase I of clinical trials [44]. This could be explained by the fact that its mode of action is based on interactions with extracellular collagen [45] and with actin-type proteins on the cell surface [46].
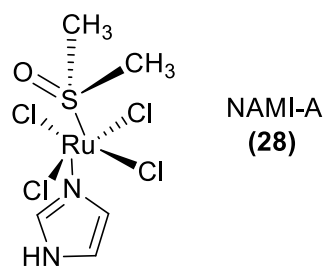
Figure. 1.24 – Structure of the ruthenium(III) complex NAMI-A

On the other hand, KP1019 (indazolium [trans-Ru(III)Cl$_4$bisindazole]) showed significant *in vitro* apoptotic activity against colorectal cancer [47] and has successfully overcome phase I clinical trials [48]. For that reason, KP1019 is currently under phase II trials.
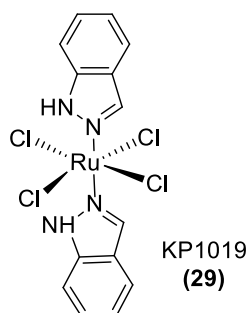
Figure. 1.25 – Structure of the ruthenium(III) complex KP1019

1.4.2. Ruthenium(II) complexes and cancer

As mentioned above, ruthenium in the +3 oxidation state is not biologically active, needing the action of compounds such as glutathione and glutamate to be reduced to its biologically active form, ruthenium(II). For that reason, many scientists believe in the therapeutic potential of ruthenium(II) complexes due to their direct activity *in vivo*, without the need of being reduced. Besides, ruthenium(II) complexes are more stable.

In the last two decades, ruthenium(II) anticancer drug candidates, both inorganic polypyridyl complexes and organometallics with arene facial ligands, were the target of several studies. One example is the RAPTA family, where RAPTA C or *[Ru(II)(η^6-p-cymene)(PTA)Cl$_2$], PTA = 1,3,5-triaza-7-phosphatricyclo-[3.3.1.1]*

decanephosphine) demonstrated the most interesting biological effect being used as a model for the design of new RAPTA compounds [49].

1.4.3.   Cytotoxicity of Ru(II) [9]aneS$_3$ complexes

Ru(II)[9]aneS$_3$ complexes ([9]aneS$_3$ = 1,4,7-trithiacyclononane) are emerging in the scientific community, and have a tridentate ligand in place of the arene [50]. Their cytotoxicity effect against PC-3 and MDA-MB-231 cells was already described by *J. Marques* and coworkers in 2014 [6].   The aim of *J. Marques* was to synthesize the complex [Ru([9]aneS3)(phpz)Cl$_2$] (phpz: 5-(2-hydroxyphenyl)-3-[(4-methoxystyryl)-1*H*-pyrazole)) inspired by the antitumor effect of pyrazole derivatives and ruthenium(II) complexes[6]. The results obtained showed that *[Ru([9]aneS3)(phpz)Cl$_2$* presented notable cytotoxic action towards the MDA-MB-231 and PC-3 human cancer cell lines when compared with the antitumor agent cisplatin [6]. However, the relationship between the selectivity of *phpz* towards cancer cells and the need of using ruthenium complexes has not yet been proved on this study, because no studies for healthy cells were made.[6].
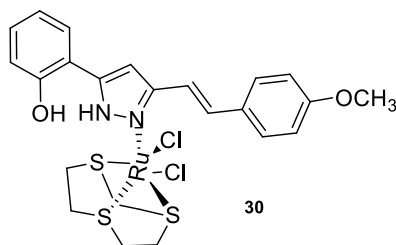
Figure. 1.26 – Structure of the complex [Ru([9]aneS3)(phpz)Cl$_2$]

Considering the results obtained by *J. Marques* we were inspired to combine others *3(5)-(2-hydroxyphenyl)-1H-pyrazoles* with ruthenium (II) complexes and study their cytotoxicity activity against tumor cell lines. In addition, based on the studies reported in the literature, we believe that the *3(5)-(2-hydroxyphenyl)-1H-pyrazoles* selected for our study can also possess antioxidant activity. Accordingly, this biological activitiy will be evaluated in due course.

2. Pyrazoles, glycosylpyrazoles, and their ruthenium complexes

2.1. Nomenclature of the compounds

This topic aims to present the structure and numeration of the synthesized compounds. The nomenclature attribution was based on IUPAC norms for some of the compounds and abbreviations for some other ones were applied and used by QOPNA.

In order to facilitate, the numeration of the compounds in this new topic will start from number 1.

2.1.1. (*E*)-3(5)-(2-hydroxyphenyl)-5(3)-arylstyryl-1*H*-pyrazoles

According to IUPAC, the numeration of (*E*)-3(5)-(2-hydroxyphenyl)-5(3)-arylstyryl-1*H*-pyrazoles (**2**) presented in the scheme 2.1, obtained from (*E*)-5-(4-chlorophenyl)-1-(2-hydroxyphenyl)pent-4-ene-1,3-dione, starts in the nitrogen covered with an hydrogen at the pyrazole nucleous and then numbering successively to the rest of the carbon chain. The pyrazole nucleous presents two tautomers in tautomeric equilibrium, due to the fact of being unsubstituted (free NH). Their abundance is relative, depending on the environment and the two structures are presented on scheme 2.1. For this present work, we decided to use the tautomer **I** to identify the RMN specters of (*E*)-3(5)-(2-hydroxyphenyl)-5(3)-arylstyryl-1*H*-pyrazoles for being the most probable.
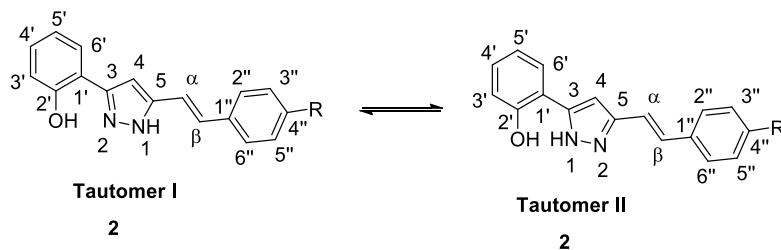
Scheme 2.1 – Structure of the (*E*)-3(5)-(2-hydroxyphenyl)-5(3)-arylstyryl-1*H*-pyrazoles (**2**) and the phenomenon of tautomeris

2.1.2. (*E*)-3(5)-(2-hydroxyphenyl)-4-arylstyryl-1*H*-pyrazoles

The numeration and nomenclature for *(E)*-3(5)-(2-hydroxyphenyl)-4-arylstyryl-1*H*-pyrazoles (**4**) followed the same rules as the ones applied to (*E*)-3(5)-(2-hydroxyphenyl)-5(3)-arylstyryl-1*H*-pyrazoles (**2**), except that the arylstyryl group changes its position to the carbon 4 of the pyrazole nucleus as depicted in the scheme 2.2.
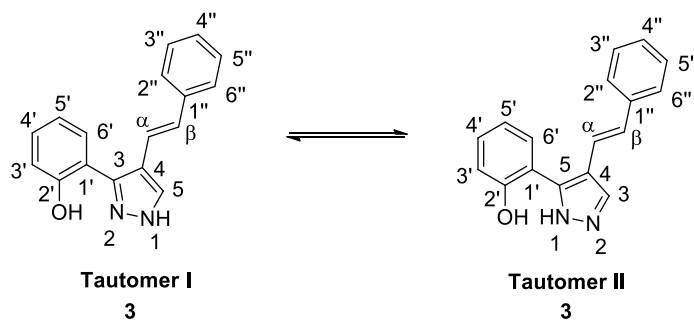
Scheme 2.2. – Structure *(E)*-3(5)-(2-hydroxyphenyl)-4-arylstyryl-1*H*-pyrazoles (**3**) and the phenomenon of tautomeris.

2.1.3. Glycosylated pyrazoles

The nomenclature and numeration of (*E*)-3(5)-[2-β-D-(2,3,4,6-tetraacetylglycosyl)phenyl]-5(3)-[2-vinyl]-1*H*-pyrazole (**5**) and (*E*)-3(5)-(2-β-D-glycosylphenil)-5(3)-[2-(4-vinyl]-1*H*-pyrazole (**6**) followed the same rules as the ones used for pyrazoles **2** and **3**, incorporating the nomenclature <'''> for the glucose monomer as depicted on figure 2.1.
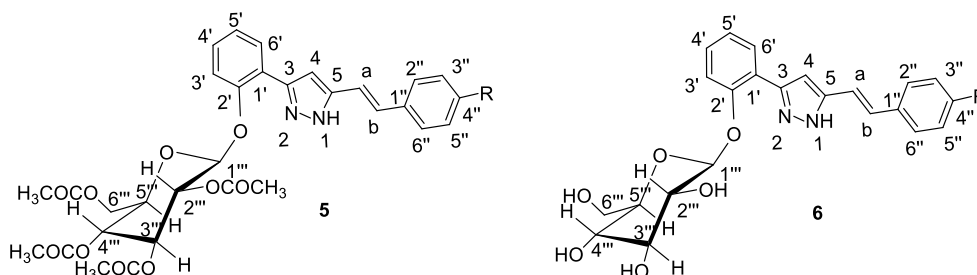
Figure 2.1 – Structure and numeration of (*E*)-3(5)-[2-β-D-(2,3,4,6-tetraacetylglycosyl)phenyl]-5(3)-[2-vinyl]-1*H*-pyrazole (**5**) and (*E*)-3(5)-(2-β-D-glycosylphenil)-5(3)-[2-(4-vinyl]-1*H*-pyrazole (**6**)

2.1.4. Ruthenium trithiacyclononane complexes

The chosen name for the complexed pyrazoles with ruthenium tritiacyclononane was Ru([9]aneS$_3$(phpz)Cl$_2$] **(8)** with phpz = (*E*)-3(5)-(2-hydroxyphenyl)-5(3)-arylstyryl-1*H*-pyrazoles. The general structure is presented on figure 2.2.
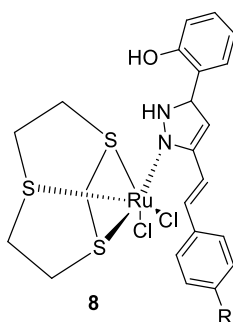
Figure 2.2 – Structure of the Ru([9]aneS$_3$(phpz)Cl$_2$] **(8)**

2.2. Synthesis and characterization

2.2.1. (*E*)-3(5)-(2-hydroxyphenyl)-5(3)-arylstyryl-1*H*-pyrazoles

(*E*)-3(5)-(2-hydroxyphenyl)-5(3)-arylstyryl-1*H*-pyrazoles **(2)** were obtained in moderate yields by treating (*E*)-5-(4-chlorophenyl)-1-(2-hydroxyphenyl)pent-4-ene-1,3-dione **(1)** with hydrazine hydrate as depicted in the scheme 2.3 and obtained in 52, 21, 58 and 34 % yield for **2a-d**, respectively.

a: R = H
b: R = Cl
c: R = NO$_2$
d: R = OCH$_3$

η = 21 %
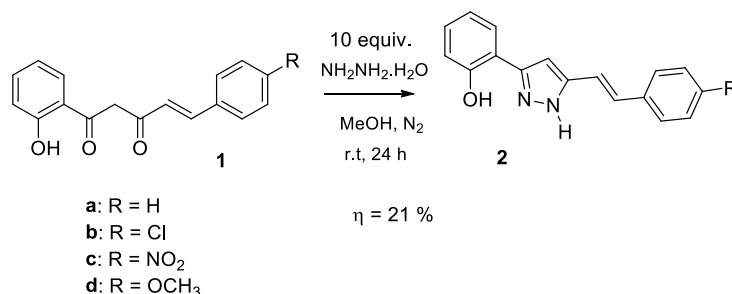
Scheme 2.3 – Synthesis of compounds of (*E*)-3(5)-(2-hydroxyphenyl)-5(3)-styryl-1*H*-pyrazoles **(2).**

The structural characterization of compounds **2a**-**2d** is already reported [51], and they were used as reference for the interpretation of 1D ^{1}H NMR and ^{13}C data for 5(3)-(4-chlorostyril)-3(5)-(2-hydroxyphenyl)pyrazole (**2b**). ^{1}H NMR spectrum of **2b** is presented in the figure 2.3. These results were confirmed in the ^{13}C NMR spectre. It is noteworthy the absence of tautomerism, as denoted by the observation of only two significant singlets for NH (9.02 ppm) and for OH (10.68 ppm) in the ^{1}H NMR spectrum. Tautomeris is a common phenomenon in pyrazoles and in *phpz* compounds (Scheme 2.1).
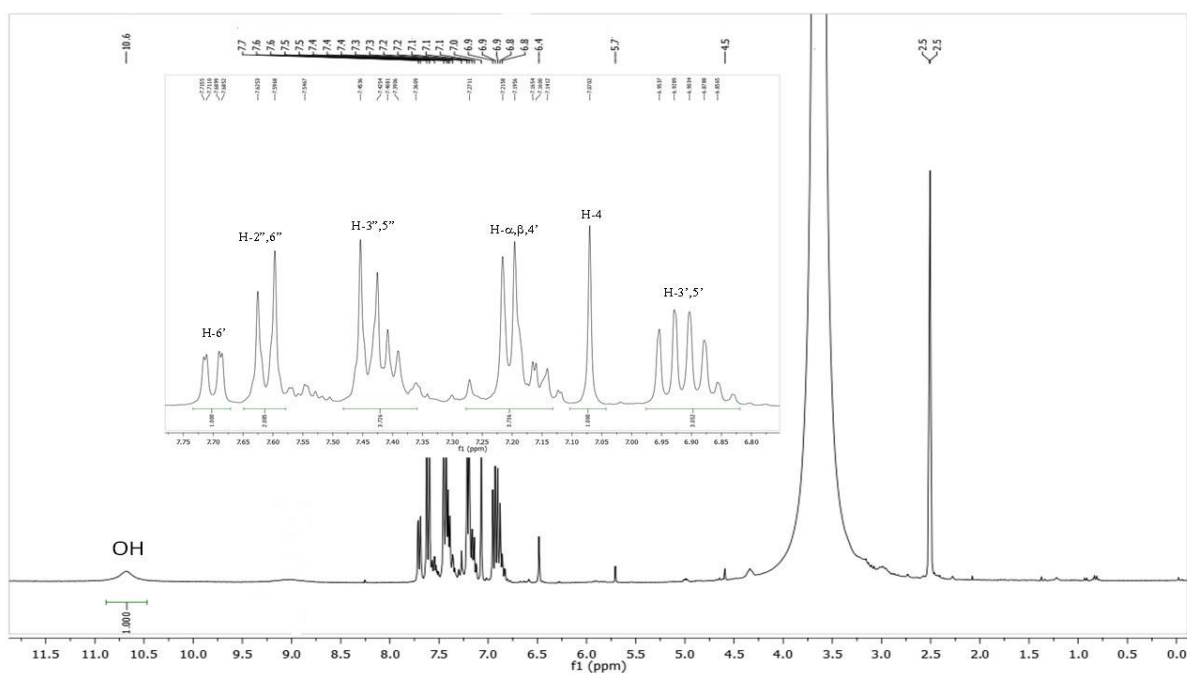
Figure 2.3 – ^{1}H NMR spectrum of (*E*)-5(3)-[2-(4-chlorophenyl)vinyl]-3(5)-(2-hydroxyphenyl)-1*H*-pyrazole (**2b**) in DMSO-*d*6

2.2.2. (*E*)-3(5)-(2-hydroxyphenyl)-4-arylstyryl-1*H*-pyrazoles

(*E*)-3(5)-(2-hydroxyphenyl)-4-arylstyryl-1*H*-pyrazoles (**4**) were obtained in moderate yields (48.3 mg; 46 %) by treating (*E*)-3-[2-(4-phenyl)vinyl]-4H-chromen-4-one (**3**) with hydrazine hydrate as depicted in the scheme 2.4.
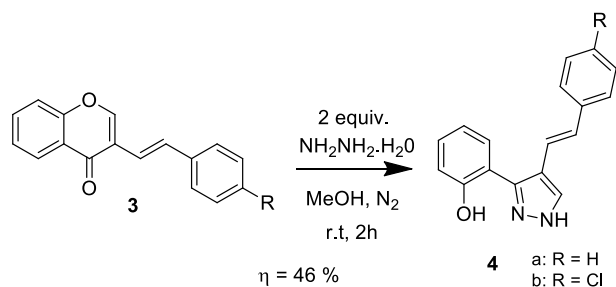
Scheme 2.4 – Synthesis of (*E*)-3(5)-(2-hydroxyphenyl)-4-styryl-1*H*-pyrazoles (**4**).

The structures of **4a** and **4b** are already reported [52], and they were used as reference for the confirmation of 1D ^{1}H NMR for *(E)*-3(5)-(2-hydroxyphenyl)-4-styryl-1*H*-pyrazoles **(4a).** The pyrazole **4b** was already synthesized and stored in the laboratory.

2.2.3. (*E*)-3(5)-(2-β-D-glycosylphenyl)-5(3)-[2-(4-methoxyphenyl)vinyl]-1*H*-pyrazole

The (*E*)-3(5)-(2-β-D-glycosylphenyl)-5(3)-[2-(4-methoxyphenyl)vinyl]-1*H*-pyrazole **(5d)** was obtained following two steps procedure as depicted in the scheme 2.5. The first step involved the reaction of pyrazole **2d** with 2,3,4,6-Tetra-O-acetyl-α-D-glucopyranosyl bromide and NaH in THF at room temperature, affording the (*E*)-3(5)-[2-β-D-(2,3,4,6-tetraacetylglycosyl)phenyl]-5(3)-[2-(4-methoxyphenyl)vinyl]-1*H*-pyrazole **(5d)** in low yields (14%). The second step is the deprotection of the sugar moiety by cleavage of the acetyl groups, which was carried out using Amberlite IRA-400 (OH) resin (which was prepared from IRA-400 (Cl) after treatment with NaOH aqueous solution, H$_2$O and MeOH) and the (*E*)-3(5)-(2-β-D-glycosylphenyl)-5(3)-[2-(4-methoxyphenyl)vinyl]-1*H*-pyrazole **(6d)** was obtained in 67.5% yield. This compound was synthesized by my colleague Sofia Brandão during the curricular unit of master project and was used for the biological tests.
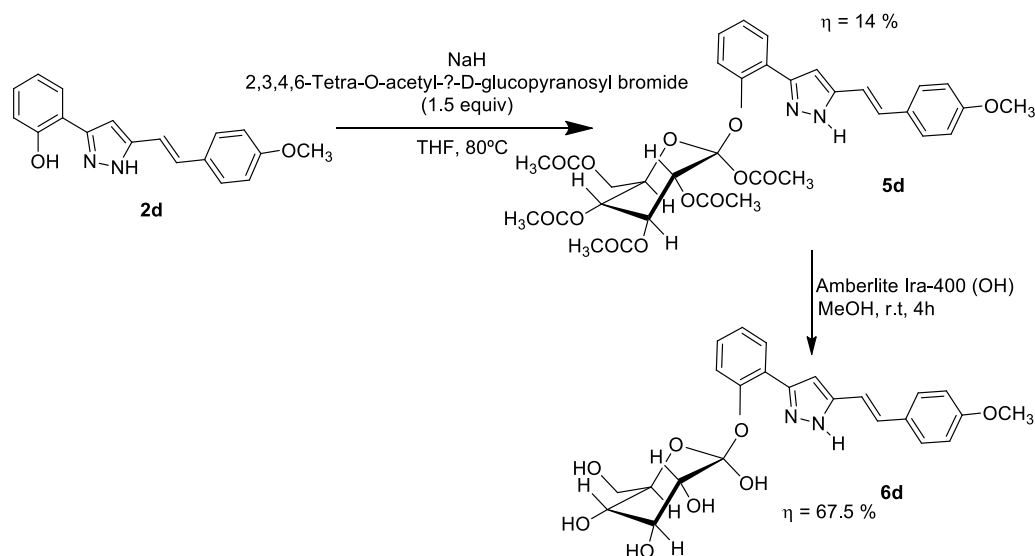
Scheme 2.5 – Synthesis of (*E*)-3(5)-(2-β-D-glycosylphenyl)-5(3)-[2-(4-methoxyphenyl)vinyl]-1*H*-pyrazole (**6d**)

It is noteworthy that other methods are being studied and developed aiming to improve the yield of the synthesis of (*E*)-3(5)-[2-β-D-(2,3,4,6-tetraacetylglycosyl)phenyl]-5(3)-[2-(4-methoxyphenyl)vinyl]-1*H*-pyrazole (**6d**).

The structure of the (*E*)-3(5)-[2-β-D-(2,3,4,6-tetraacetylglycosyl)phenyl]-5(3)-[2-(4-methoxyphenyl)vinyl]-1*H*-pyrazole (**5d**) was elucidated by 1D ^{1}H and ^{13}C NMR, relying on 2D techniques (^{1}H–^{13}C HSQC, HMBC and NOESY) for the unambiguous assignment of a few resonances. By comparison of these spectra with the spectrum of (*E*)-3(5)-(2-hydroxyphenyl)-5(3)-[2-(4-methoxyphenyl)vinyl]-1*H*-pyrazole (**2d**) we observed, the disappearance of the singlet of the OH in the ^{1}H NMR spectrum of **5d** (Figure 2.4) that can be indicative of the presence of the glucose unity linked to the oxygen. This suspicion was confirmed by the correlation found in the HMBC spectrum (H-1'''→ C-2') Furthermore, the appearance of new signals at 4.0-6.0 e a 1.2-2.1 ppm are due to the resonances of the protons of the glucose unit and of the acetyl protecting groups, respectively.
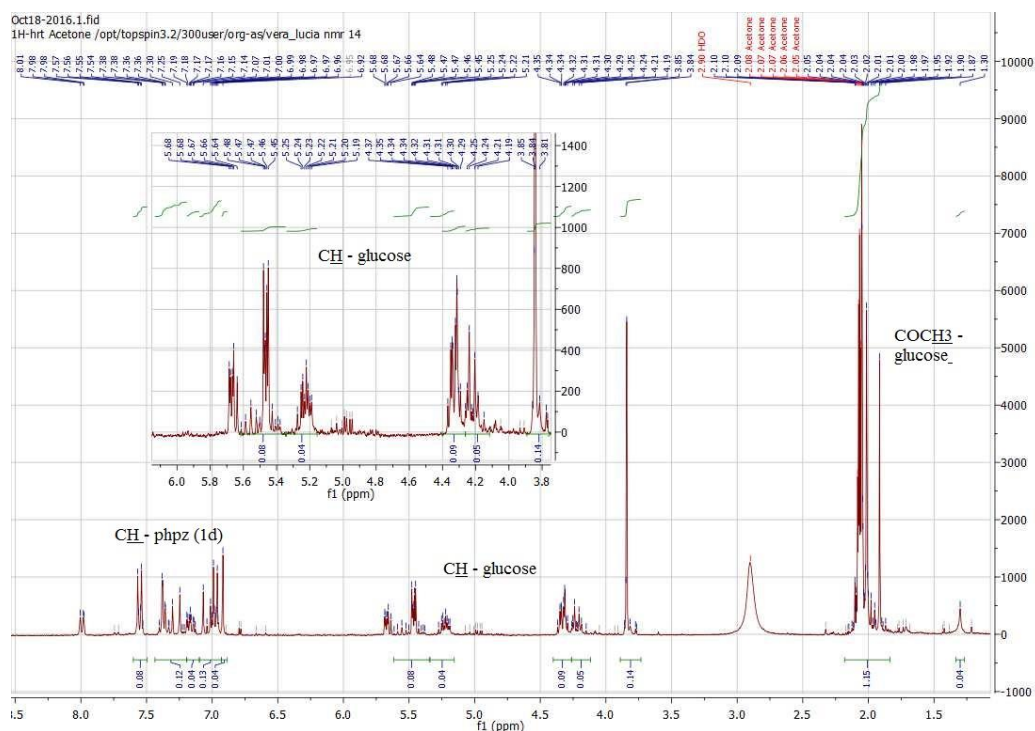
Figure 2.4 – Spectrum of ^{1}H NMR in $(CD3)_3CO$ of (*E*)-3(5)-[2-β-D-(2,3,4,6-tetraacetylglycosyl)phenyl]-5(3)-[2-(4-methoxyphenyl)vinyl]-1*H*-pyrazole **(5d).**

The ^{13}C NMR spectrum of (*E*)-3(5)-[2-β-D-(2,3,4,6-tetraacetylglycosyl)phenyl]-5(3)-[2-(4-methoxyphenyl)vinyl]-1*H*-pyrazole (**5d**) (Figure 2.5) indicates the appearance of new signals, due to the resonances of the carbons of the glucose unity, at 62.9-98.6 ppm. The carbonylic carbons of the acetyl groups (COCH3) appears at 169.9-170.7 ppm and the carbons of the methyl of the protecting groups (COCH3) at 20.5-20.8 ppm.
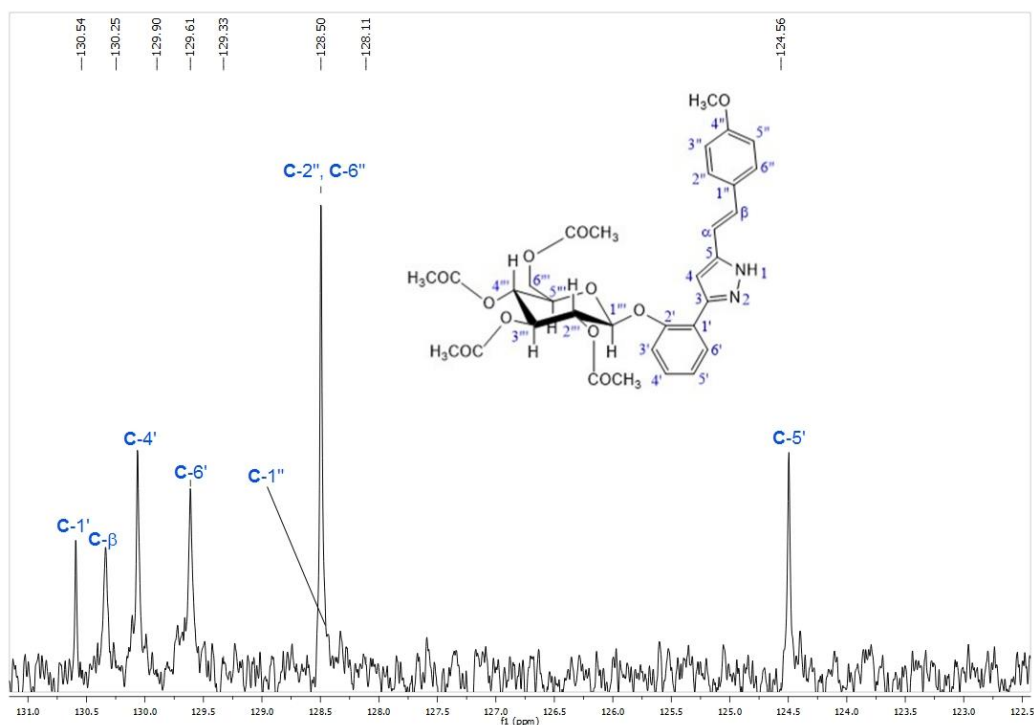
Figure 2.5 – Spectrum of the ^{13}C NMR in $(CD3)_3CO$ of (E)-3(5)-[2-β-D-(2,3,4,6-tetraacetylglycosyl)phenyl]-5(3)-[2-(4-methoxyphenyl)vinyl]-1H-pyrazole **(5d).**

The structure of the (E)-3(5)-(2-β-D-glycosylphenyl)-5(3)-[2-(4-methoxyphenyl)vinyl]-1H-pyrazole **(6d)** was unequivocally identified by 1D ^{1}H NMR and ^{13}C NMR, based on 2D techniques (^{1}H–^{13}C HSQC, HMBC and NOESY) and based on the comparison with the spectrum of the (E)-3(5)-[2-β-D-(2,3,4,6-tetraacetylglycosyl)phenyl]-5(3)-[2-(4-methoxyphenyl)vinyl]-1H-pyrazole **(5d).** Looking at ^{1}H NMR, it was possible to see the absence of the signals due to the resonance of the protons of the acetyl groups that appeared at 1.2 to 2.1 ppm in the spectrum of **5d**, thus indicating that the cleavage of these groups was successfully achieved (Figure 2.6). The analysis of the ^{13}C NMR spectrum of the pyrazole **6d** also confirmed the disappearance of the signals due to the resonance of the carbons of the acetyl groups (COCH$_3$ and COCH$_3$) (Figure 2.7).
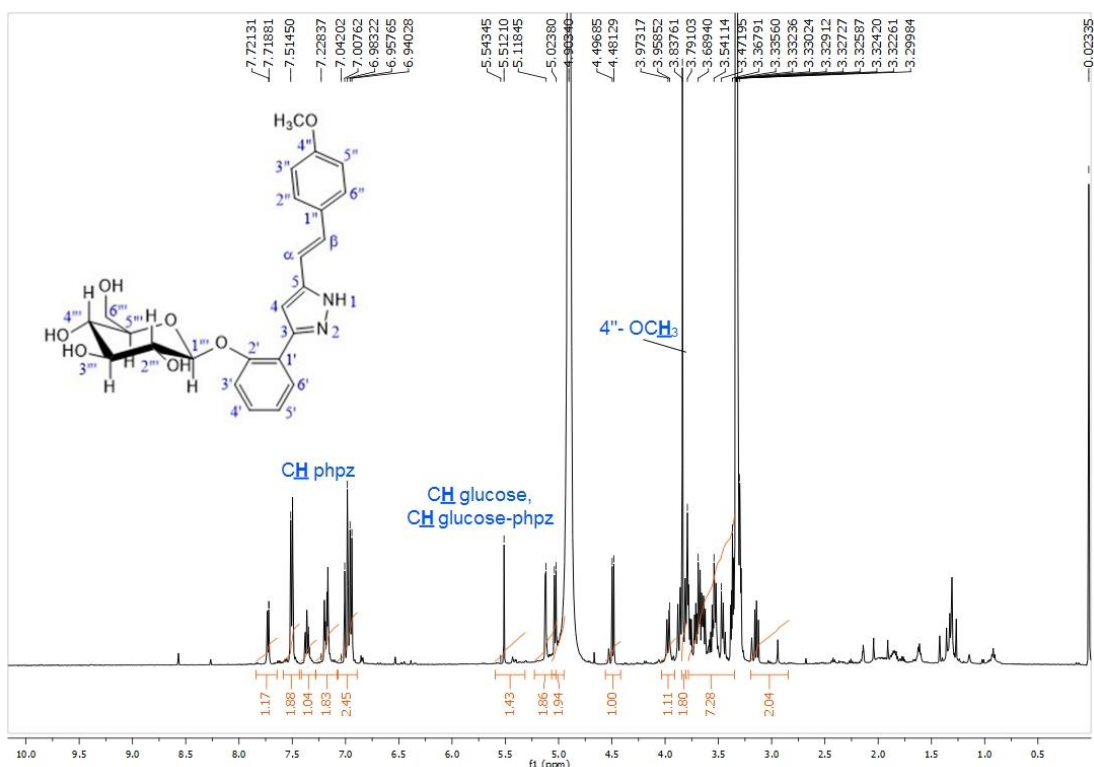
Figure 2.6 – Full ^{1}H NMR spectrum in (CD3)$_3$CO of (*E*)-3(5)-(2-β-D-glycosylphenyl)-5(3)-[2-(4-methoxyphenyl)vinyl]-1*H*-pyrazole **(6d).**
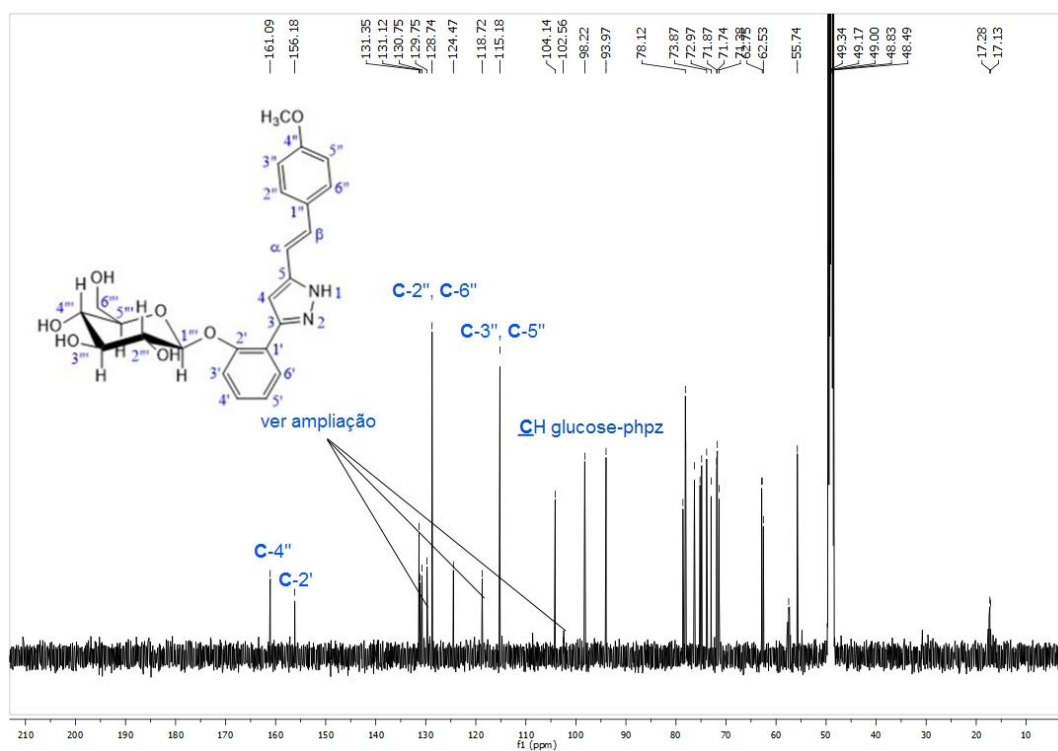
Figure 2.7 – Full ^{13}CNMR spectrum in (CD3)$_3$CO of (*E*)-3(5)-(2-β-D-glycosylphenyl)-5(3)-[2-(4-methoxyphenyl)vinyl]-1*H*-pyrazole **(6d).**

2.2.4. Ruthenium trithiacyclononane complexes

Ruthenium trithiacyclononane complexes (**8**) were obtained in moderate yields, c.a. 47.4 %, by treating *phpz* with Ru([9]aneS$_3$)(DMSO)Cl$_2$ (**7**), as depicted in the scheme 2.6. This method was an adaptation of the one used by *J. Marques et al*. [53], using as solvent ethanol, for to be less toxic.
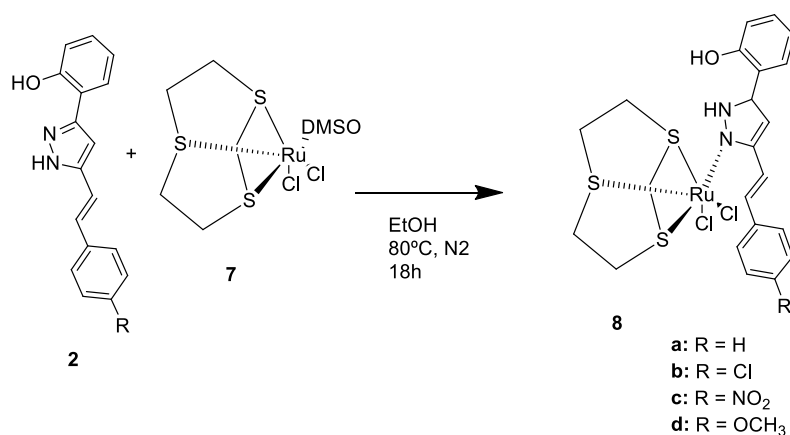
Scheme 2.6 - Representation for the functionalization of **2** with Ru([9]aneS$_3$)(DMSO)Cl$_2$ (**7**).

The ^{1}H NMR spectrum of **8b** is well-demonstrative of the effects of metal coordination (Figure 2.8). The resonance of NH appears shifted from $\delta \sim 9.02$ ppm to 12.89 ppm, typical for the coordination between N2 of the free *phpz* and the ruthenium cation. The signal for the OH of the coordinated *phpz*, unlike the free ligand, is now at lower values than those of the NH, also due to the coordination effect.
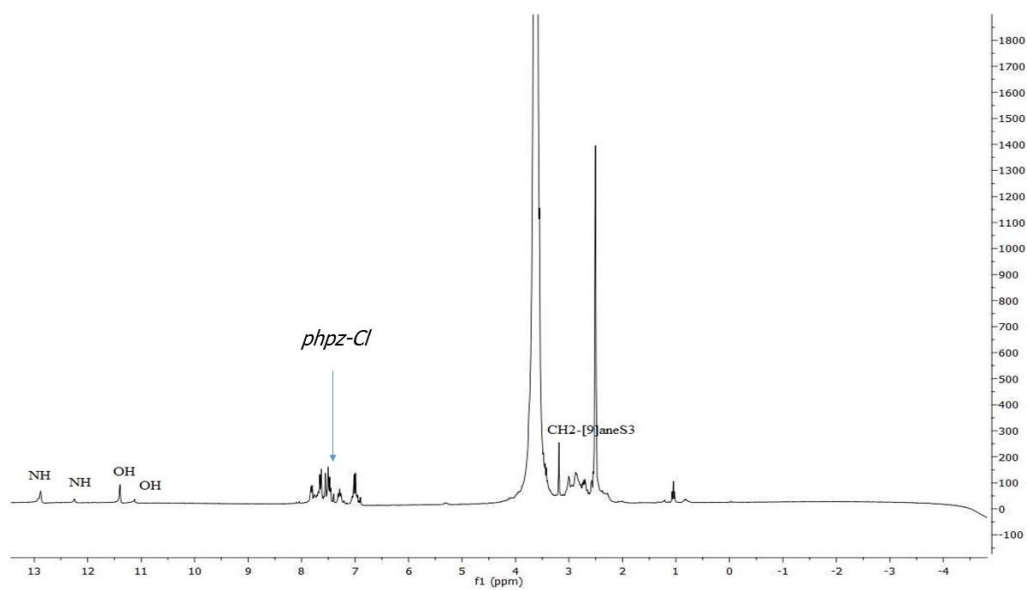
Figure 2.10 – Total ^{1}H NMR spectrum of Ru([9]aneS$_3$)(phpz-Cl)Cl$_2$ **(8b)** in DMSO-d_6

3. Biological tests

3.1. Antioxidant activity

3.1.1.   NO scavenging assay

The antioxidant activity of the pyrazoles **2a-2d** and **4** (Chapter 2) were tested using the NO scavenging assay, a discoloration method based on the reduction of nitric oxides that are generated by the conversion of sodium nitroprusside to nitrous acid by air contact. These oxides can diazotize with 4-aminobenzenesulfonamide and couple with Griess reagent (naphthylethylenediamine) producing pink color that can be measured at 546 nm, as depicted in the scheme 3.1.
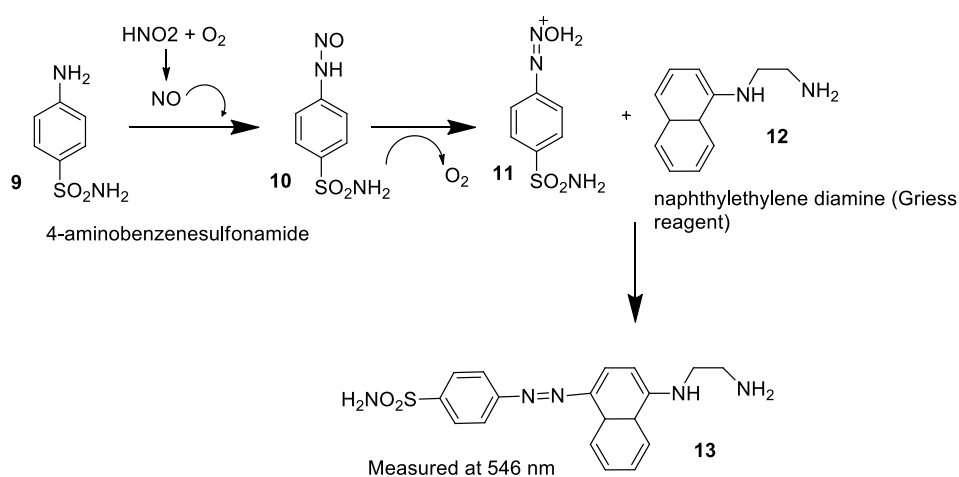
Scheme 3.1 – NO Scavenging assay: Diazotization of nitric oxides with 4-aminobenzenesulfonamide and consequently coupling with Griess Reagent, a product that can be measured at 546 nm.

This test is very important not only to achieve the antioxidant activity by pyrazoles, but also the anti-inflammatory action, once nitric oxide is a pleitropic mediator of inflammation and responsible for several issues such as oxidative DNA damage, dysregulation of apoptosis, oncogene expression, etc. Because of that, having a compound responsible for the reduction of nitric oxides, could be a possible way to reduce chronic inflammation and consequently help preventing cancer. However, due to the weak solubility of compounds **2a-d** and **4b** on water and the respective use of aqueous buffer

solutions we weren't able to prepare quantifiable dilutions to this method, since higher concentrations always precipitated.

The protocol for this assay relays on the preparation of potassium phosphate buffer, sodium nitroprausside, ascorbic acid and griess reagent solutions and is described on chapter 4.

3.1.2. 2,2'-azino-bis(3-ethylbenzothiazoline-6-sulphonic acid) (ABTS) assay

The antioxidant activity of the pyrazoles of compounds **2a-d** and **4b** (Chapter 2) was tested using the ABTS assay, a decolorization method based on the reduction of the radical monocation 2,2′-azinobis-(3-ethylbenzothiazoline-6-sulfonic acid) (ABTS$^{\bullet+}$), that is generated by oxidation of ABTS with potassium persulfate (measured at 734 nm) and reduced in the presence of such hydrogen-donating antioxidants (as depicted in the scheme 3.2). Glycopyrazole **6a** (Chapter 2) was also tested in order to understand if the glucose monomer as influence in the radical scavenging.
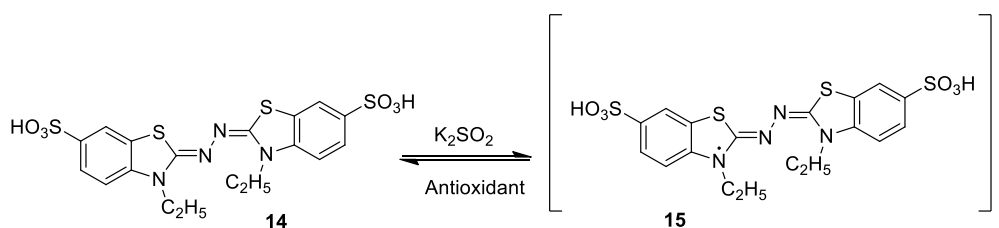
Scheme 3.2 - Oxidation of ABTS with potassium persulfate and reduction in the presence of such hydrogen-donating antioxidants.

Unlike NO scavenging, this method provide debatable results, by diluting our solutions in 10% DMSO and 90 % methanol (percentages that did not interfere with the assay). For that reason, we were able to identify some structure-activity relationship between compounds **2a-d** and **4b**. The introduction of a glucose monomer, unlike our expectations, did not present benefits in the radical scavenging activity. These results are presented on chapter 5 and the protocol is described on chapter 4.

3.1.3.　Beta-carotene assay

The antioxidant activity of the pyrazoles of compounds **2a-d** and **4b** (Chapter 2) was tested for Beta-Carotene assay, a decolorization method based on the oxidation of beta-carotene by linoleic acid (measured at 470 nm) and its respective protection by antioxidants.

After several attempts, compounds **2a-b**, **2d** and **4b** did not display remarkable antioxidant activity percentages. Pyrazole **2c** was the only one presenting a maximum percentage of antioxidant activity above 60 %, for 12.5 µg/mL. However, these values did not follow a typical linearity capable of calculating the IC_{50} for pyrazole **2c** on the beta-carotene assay.

3.2. Cytotoxic and Cytostatic Activity

3.2.1.　MTT assay

The cytotoxic activity of the pyrazoles of compounds **2a-d** and **4a** (Chapter 2) was tested for the MTT assay, a colorimetric assay for accessing cell metabolic activity by the reduction of MTT 3-(4,5-dimethylthiazol-2-yl)-2,5-diphenyltetrazolium bromide to its insoluble formazan (purple color and measured at 570 nm). This reduction is caused by the action of NAD(P)H-dependent cellular mitochondrial oxidoreductase enzymes and is depicted in the scheme 3.3.
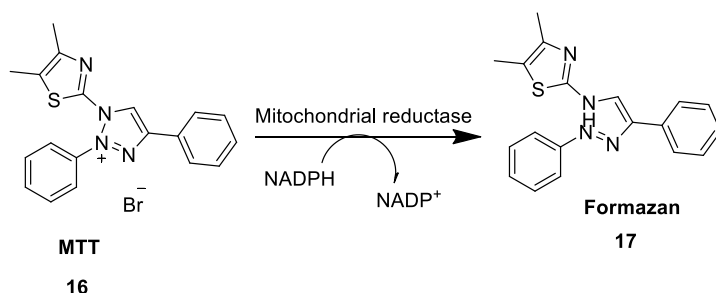
Scheme 3.3 – Reduction of the MTT to its insolube formazan by the mitochondrial NAD(P)H-dependent cellular oxidoreductase.

Due to previous results obtained for [Ru([9]anoS$_3$(phpz-OCH$_3$)Cl$_2$] complex [53], we decided to introduce the new [Ru([9]anoS$_3$(phpz)Cl$_2$] complexes **8a** and **8b**, in order to understand how ruthenium complexes can possibly affect the cytotoxicity effect and either the selectivity for tumor cell lines. New glycosylpyrazole **6a** due to its glucose monomer, was selected to study their selectivity for tumor cell lines, in the case of successful cytotoxicity from free *phpz*. However, for reasons of time, this last test has never been made.

3.2.2.   DNA Intercalation Studies

The cytostatic activity of pyrazole **8b** was tested by the DNA intercalation study, based on the calculous of the DNA denaturation temperature (measured at 260 nm). This result was compared to the one previously studied, pyrazole **8d.**

4. Experimental procedures

4.1. Chemicals, solvents and methods

The reagents hydrazine hydrate, 2,3,4,6-Tetra-*O*-acetyl-α-D-glucopyranosyl bromide and NaH were obtained from Sigma-Aldrich.

Amberlite Ira-400 (OH) was obtained from Amberlite Ira-400 (Cl) by ion exchange.

Dichloromethane was dried by reflux with calcium hydride, followed by distillation and stored in a recipient with molecular sieves. THF was dried in a metallic wire of sodium, heated in reflux in nitrogen atmosphere, using benzofenone as indicator, distillated in the hotte and collected to an erlenmeyer with molecular sieves. The other solvents namely chloroform, acetone, acetonitrile, ethanol, methanol, anhydrous sodium sulfate and diethyl ether were of analytical grade.

Ascorbic acid, α-Tocopherol, 2,2′-azinobis-(3-ethylbenzothiazoline-6-sulfonic acid) (ABTS•+) and potassium persulfate were obtained from Sigma-Aldrich.

Absorbance measures were carried out in one EON BIOTEK plate reader for ABTS, NO and Beta-Carotene assays and MTT assay; and UV-Vis GBC Sintra 303 for DNA intercalation studies.

1D (^{1}H and ^{13}C) and 2D (^{1}H–^{13}C HSQC and HMBC) NMR spectra were recorded at ambient temperature in a Bruker Avance 300 (frequencies: 300.13 MHz for ^{1}H, 75.47 MHz for ^{13}C) or in a Bruker DRX 500 spectrometer (500.13 MHz for ^{1}H and 125.76 MHz for ^{13}C). Chemical shifts are quoted in parts per million (ppm) and coupling constants (*J*) are indicated in Hz..

Mass spectra were recorded in a Micromass® Q-ToF 2 mass spectrometer.

4.2. Protocols
4.2.1. Synthesis of 3(5)-(2-hydroxyphenyl)-5(3)-styryl-1*H*-pyrazoles (2)

The synthetic procedure for the preparation of *phpz* compounds [51] is represented in the scheme 2.3. Compound **2b** was prepared freshly following this procedure. A solution of (*E*)-5-(4-chlorophenyl)-1-(2-hydroxyphenyl)pent-4-ene-1,3-dione (413.3 mg ; 1.37 mmol) in methanol (100 mL) was treated with 10 equiv. of hydrazine hydrate (0.70 mL, 13.7 mmol) and the solution was left at ambient temperature with stirring for 24h under

nitrogen atmosphere. After that period the reaction mixture was concentrated at reduced pressure to evaporate the methanol partially, chloroform was added to the reaction mixture and it was washed with acidified water. Then the organic layer was dried over anhydrous sodium sulfate and the solvent was removed. Note that compounds **2a, 2c** and **2d** were already available in the laboratory and only compound **2b** was prepared freshly. It was isolated as a pale yellow solid, matching the colour of the remaining *phpz* compounds. The yield for compound **2b** was of 84.5 mg (~21%), slightly lower than the values reported for this family of compounds. The yields for **2a, 2c** and **2d** were 52%, 58% e 34% [50], respectively.

(*E*)-5(3)-[2-(4-chlorophenyl)vinyl]-3(5)-(2-hydroxyphenyl)-1*H*-pyrazole (2b)

^{1}H NMR (300.13 MHz, DMSO-d$_6$): δ(ppm) = 6.87-6.95 (3'-H and 5'-H, m), 7.07 (s, 1H, 4-H), 7.14-7.22 (Hα, Hβ and 4'-H, m), 7.43 (3''-H and 5''-H, d, 8.6 MHz), 7.61 (2''-H and 6''-H, d, *J* = 8.6 MHz), 7.70 (6'-H, dd, *J* = 1.4, 7.7 MHz), 10.68 (s, 1 H, 2'-OH), 9.02 (s, 1H, NH).

^{13}C NMR: δ (ppm) = 116.6 (C-3'), 129.2 (C'4), 117.0 (C-1'), 118.2 (C-α), 119.6 (C-5'), 127.2 (C-6'), 128.4 (C-2'), 128.4 (C-2'',6''), 129.1 (C-3'',5''), 129.2 (C-4'), 129.3 (C-β), 132.6 (C-4''), 135.6 (C-1''), 144.4 (C-5), 148.0 (C-3),

Figure 4.1 - Atom labelling scheme for (*E*)-5(3)-[2-(4-chlorophenyl)vinyl]-3(5)-(2-hydroxyphenyl)-1*H*-pyrazole **(2b)**

4.2.2. Synthesis of (*E*)-3(5)-(2-hydroxyphenyl)-4-arylstyryl-1*H*-pyrazoles

Pyrazoles **4a** and **4b** were already mentioned in the literature [52]. Pyrazole **2a** was already available in the laboratory and pyrazole **4b** was needed to synthesize more quantities.

A solution of 3-(2-phenyl)vinyl-4*H*-chromen-4-one. (100.0 mg, 0.403 mmol) in methanol (50 mL) was treated with 2.0 equiv. of hydrazine hydrate (0.50 mL, 0.806 mmol) and the solution was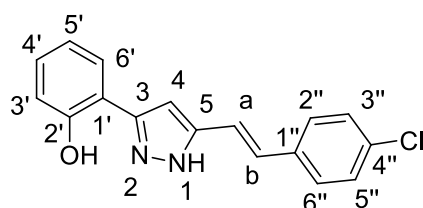 left at ambient temperature with stirring for 2h under nitrogen atmosphere. It was isolated as a pale white solid and the yield for compound **4b** was of 48.3 mg (~46%).

4.2.3. Synthesis of (*E*)-3(5)-[2-β-D-(2,3,4,6-tetraacetylglycosyl)phenyl]-5(3)-[2-(4-methoxyphenyl)vinyl]-1*H*-pyrazole (5d)

To a solution of **2d** (200.0 mg; 0.684 mmol) in THF (20 mL) were added 2.0 equiv. of NaH (33.92 mg; 1.414 mmol) and 3.0 equiv. of 2,3,4,6-Tetra-*O*-acetyl-α-D-glucopyranosyl bromide (845.49 mg; 2.06 mmol). The mixture was stirred at 80 ºC using Schlenk techniques and left for 6 days. After that period, the mixture was filtered with cannula and a beige solid together with a yellow liquid was obtained. The solution was purified by thin layer chromatography with CH_2Cl_2/Acetone (9:1) and affording 14.4 % for **5d** (61.3 mg; 0.0984 mmol). The chemical shifts (δ) are reported in ppm among with the coupling constants (J) in MHz that were collected by my colleague Sofia in the curricular unit of master project.

(*E*)-3(5)-[2-β-D-(2,3,4,6-tetraacetylglycosyl)phenyl]-5(3)-[2-(4-methoxyphenyl)vinyl]-1*H*-pyrazole (6d)

^{1}H NMR (500.13 Hz, CD_3O): δ(ppm) = 6.96 (d, 2H, *J* = 8.7 Hz, H-3", H-5''), 07.09 (s, 1H, H-α); 7.01 (s, 1H, H-4), 7.21 (m, 1H, *J* = 7.6, 7.1 and 1.1 Hz, H-5'); 7.37 (dt, 1H, J = 8.2, 7.1 e 1.6 Hz, H-4'), 7.79 (dd, 1H, *J* = 7,6 and 1,6 Hz, H-6'); 7.53 (d, 2H, *J* = 7,6 Hz, H-2", H-6"); 7.50 (s, 1H, *J* = 8.2 and 1.1 Hz, H-3');; 6.96 (d, 2H, *J* = 8.7 Hz, H-3", H-5");

4.01 – 6.01 (m, 7H, CH aliphatic-glucose); 3.83 (s, 3H, 4" – OCH$_3$); 1.21 – 2.10 (s, 12H, 4 × COCH$_3$ glucose), see atom labelling scheme below.

^{13}C NMR (125.77 MHz, CD$_3$DO): δ (ppm) = 20,5 – 20,8 (4 x CO$\underline{C}$H$_3$ glucose); 55,6 (4"- O$\underline{C}$H$_3$); 62,9 – 98,6 ($\underline{C}$H alifáticos-glucose); 103,6 (C-4); 115.0 (C-3", C-5"); 118.8 (C-3'); 124.5 (C-5'); 128.5 (C-1", C-2"); 129.6 (C-6'); 130.1 (C-4'); 130.1 (C-4'); 130.3 (C-β); 130.6 (C-1'); ~145.0 (C-3, C-5); 155.5 (C-2'); 160.5 (C-4"); 169.9 – 170.7 (4 x COCH$_3$ glucose)
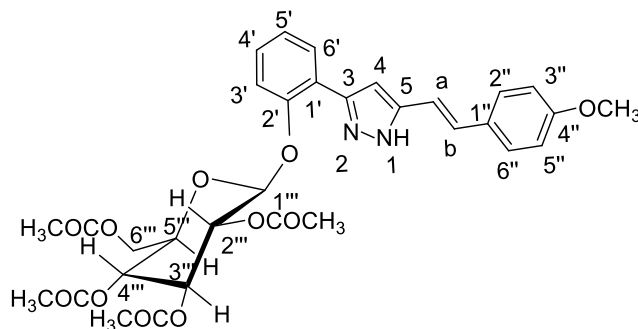
Figure 4.2 - Atom labelling scheme for (*E*)-3(5)-[2-β-D-(2,3,4,6-tetraacetylglycosyl)phenyl]-5(3)-[2-(4-methoxyphenyl)vinyl]-1*H*-pyrazole **(5d)**

4.2.4. Preparation of (E)-3(5)-(2-β-D-glycosylphenil)-5(3)-[2-(4-metoxyphenyl)vinyl]-1*H*-pirazole (6d)

The clivage of the acetyl groups in **5d** was achieved using a common method for the desprotection of sugars, using a commercial resin, Amberlite® Ira-400(OH). However, this ion-exchange resin was not available on the laboratory, only having Amberlite® Ira-400(Cl) being necessary a treatment before use. Under vacuum, a 3 mL NaOH solution (1M and pH ~ 14), together with 4 mL of water and 3 mL of methanol have been added to the resin, 1 mL portions at time. To a solution of (*E*)-3(5)-[2-β-D-(2,3,4,6-tetraacetylglycosyl)phenyl]-5(3)-[2-(4-methoxyphenyl)vinyl]-1*H*-pyrazole **(5d)** (61,3 mg; 0,0984 mmol) in 12 mLof methanol it was added Amberlite® Ira-400(OH) (61,3 mg). The procedure is carried out at room temperature and smooth magnetic agitation in methanol for about 4 h. After that time, using TLC CH$_2$Cl$_2$/Acetone (9:1) the identification of the unprotected sugar was observed and a purification was made by filtrating the resin in a filtration unity and washed with methanol. The desired product was obtained as a yellow solid in a good yield (30,2 mg; 0,066 mmol, 67.5%). The chemical shifts (δ) are reported in ppm among with the coupling constants (J) in Hz.

Note that due to time restrictions, this procedure was not applied to compound **5a**, staying for future work.

(E)-3(5)-(2-β-D-glycosylphenil)-5(3)-[2-(4-metoxyphenyl)vinyl]-1H-pirazole (6d)

EM-ESI⁺ (MeOH): *m/z* (%) = 455 (M+H)⁺ (100); 477 (M+Na)⁺ (7.72); 909 (2M+H)⁺ (3.70).

¹H NMR (500.13 Hz, CD₃O): δ(ppm) = 3.84 (s, 3H, 4" – OCH3), 4.48 (d, 3H, *J* = 7.8 Hz, CH aliphatic-glucose); 5.03 (d, *J* = 7,8 Hz, CH aliphatic-glucose); 5.12 (d, J = 3.6 Hz, CH aliphatic-glucose); 6.95 (d, 2H, *J* = 8.6 Hz, H-3", H-5"); 6.99 (d, 1H, *J* = 16.4 Hz, H-α); 6.98 (s, 1H, H-4); 7.16 – 7.20 (d, 1H, *J* = 16.4 Hz, H-β); 7.16 – 7.20 (m, 2H, H-3', H-5'); 7.36 (ddd, 1H, *J* = 7.9 e 1.4 Hz, H-4'); 7.50 (d, 2H, *J* = 8.6 Hz, H-2", H-6"); 7.73 (dd, 1H, J = 7.1 e 1.4 Hz, H-6');

¹³C NMR (125,77 MHz, CD₃DO: δ (ppm) = 55.7 (4"- OCH3); 94.0 – 104.1 (CH aliphatic-glucose); 118.7 (C-1"); 115.2 (C-3", C-5"); 128.7 (C-2", C-6"); 130.8 (C-4'); 131.1 (C-β); 131.3 (C-3', C-5'); 156.2 (C-2'); 161.1 (C-4").
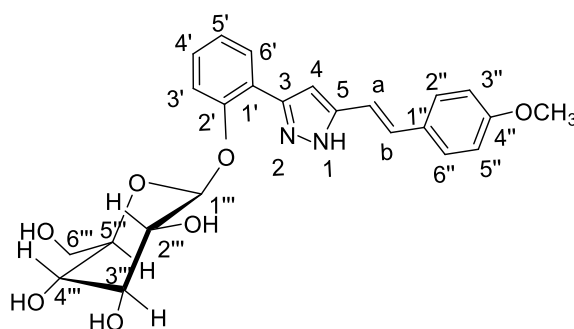
Figure 4.3 - Atom labelling scheme for (*E*)-3(5)-(2-β-D-glycosylphenil)-5(3)-[2-(4-metoxyphenyl)vinyl]-1H-pirazole **(6d)**

4.2.5. Preparation of [Ru([9]aneS$_3$(phpz-H)Cl$_2$] (8b)

[Ru([9]aneS$_3$)(phpz-Cl)Cl$_2$] complex (**8b**) was prepared by adaptation of a literature method [53].

A dry ethanol (14 mL) solution of [Ru([9]aneS$_3$)(DMSO)Cl$_2$] (55.6 mg, 0.12 mmol) and phpz-Cl (**2b**) (35.5 mg, 0.12 mmol) was refluxed, under nitrogen and using Schlenk techniques, for c.a. 18 h to afford a pale yellow precipitate. The solid was filtered, washed with 25 mL diethyl ether and dried. Yield: 36.85 mg (47.4%).

[Ru([9]aneS$_3$)(phpz-Cl)Cl$_2$]

Anal. Calc. for (C$_{17}$H$_{13}$N$_2$OCl)(RuS$_3$C$_6$H$_{12}$)Cl$_2$(H$_2$O) (648.0) (%): C, 41.45; H, 4.09; N, 4.21; S, 14.40. Found: C, 38.00 ; H, 4.11; N, 4.29; S, 14.60

ESI$^+$-MS (EtOH) *m/z* (relative intensity %): 613.0 ([Ru([9]aneS$_3$–CH$_2$CH$_2$)(phpz-Cl)]$^+$).

^{1}H NMR (300.13 MHz, DMSO-d$_6$): δ (ppm) = 2.51-3,55 (CH$_2$-[9]aneS$_3$, m); 12.89 (NH,s), 11.40 (2'-OH, s); 6.90-7.05 (H-3' and H-5', m); 7.26-7.32 (Hβ, m); 7.49 (H-3''and H-5'', d, J = 8.4 MHz); 7.55 (H-4, s); 7.65 (H-2''-H6'', d, J = 8.4 MHz); 7.72 (Hα, m), 7.65 (H-2''-H6'', d, J = 8.4 MHz),

^{13}C NMR (75 MHz, DMSO-d$_6$): δ(ppm) = 30.9; 32.5; 32.9; 33.9; 34.3; 39.8; 43.9 (CH$_2$-[9]aneS$_3$); 101.4 (C-4), 120.3 (C-5'); 113.6 (C-3'); 116.6 (C-1'); 120.3 (Cα); 128.5 (C-2''); 128.5 (C-6''); 129.1 (C-3''); 129.1 (C-5''); 130.9 (C-4'127.6 (C-6'); 133.1 (Cβ); 133.1 (C-1''); 135.5 (C-4''); 143.9 (C-5); 154.4 (C-2'); 154.0 (C-3).
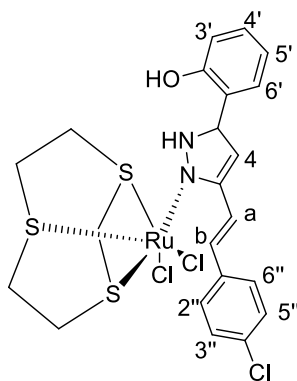
Figure 4.4 - Atom labelling scheme for [Ru([9]aneS$_3$)(phpz-Cl)Cl$_2$] (**8b**)

4.2.6. NO scavenging assay

A potassium phosphate buffer (100 Mm) was prepared by solubilizing 13.61 g of potassium phosphate in 800 mL of water and the pH was adjusted to 7.4 with NaOH (2 M). The solution was transferred to a flask and the volume adjusted to 1 L.

Sodium nitroprausside (SNP) 3.33 mM solution was prepared by solubilizing 5 mg 10 mL of potassium buffer (100 mM).

Stock solutions of test compounds **2** and **4b** (2.0 mg/mL) and the standard ascorbic acid, were daily freshly prepared in buffer and fresh working solutions were prepared using the same solvent.

Griess reagent was prepared by mixture of Griess A and Griess B (3 mL each), already prepared by dissolving 1 g of 4-aminobenzenesulfonamide in 100 mL of phosphoric acid 5% (Griess A) and 0.1 g of *N*-(1-naphthyl)ethylenediamine dihydrochloride in 100 mL of water (Griess B). Both stable at 4ºC and protected from light.

Test solutions comprised 100 µl standard or sample + 100 µl SNP solution and 100 µl Griess reagent in a 96 well-plate, incubated in the dark for 10 min and then read for absorbance at 562 nm. Three independent assays, each with a duplicate for the test samples and the appropriate solvent blank, were conducted. However, the poor solubility of pyrazoles **2a-d** and **4b** in water, caused their precipitation whenever the buffer was added. Different approaches were tried, such as dissolving the pyrazoles in DMSO. However, the addiction of SNP (prepared in buffer) and Griess (prepared in water) continued to precipitate the compounds.

4.2.7. 2,2'-azino-bis(3-ethylbenzothiazoline-6-sulphonic acid (ABTS) assay

Solutions of ascorbic acid (0.25 mg/mL) and α-tocopherol (0.25 mg/mL) were prepared in 10 mL of 10% DMSO + 90% methanol for use as stock standards. Fresh working standards were prepared daily on dilution with 10% DMSO + 90% methanol.

Stock solutions of test compounds (0.25 mg/mLwere prepared in 10% DMSO + 90% methanol and fresh working solutions were prepared daily using the same solvent for the introduction into the assay system. Methanol does not interfere in the assay, however, higher percentages of DMSO showed some significant interference.

ABTS was dissolved in water to a 7 mM concentration and the radical cation, $ABTS^{\cdot+}$, was produced by reacting ABTS stock solution with 2.45 mM potassium persulfate (final concentration) and allowing the mixture to stand in the dark at room temperature for 12– 16 h before use. After dark incubation, the absorbance at 734 nm was measured and the ABTS solution was diluted in water so that its absorbance values were within the 0.700- 0.800 interval.

Test solutions comprised 50 µl standard or sample + 250 µl ABTS solution (in a 96 well-plate), incubated in the dark for 20 min and then read for absorbance at 734 nm. Three independent assays, each with a duplicate for the test samples and the appropriate solvent blank, were conducted.

Unlike NO scavenging, this test was successful due to preparation of solutions in 10% of DMSO and the fact that for ABTS, the standard concentrations needed are lower.

4.2.8. Beta-carotene assay

A solution of beta-carotene was prepared dissolving 5 mg of beta-carotene in 5 mL of chlorophorm in a round bottom flask, keeping in dark conditions.

The beta-carotene/linoleic acid emulsion was prepared in another round bottom flask it was added 5 mg of linoleic acid, 200 mg of Tween and 1 mL of the beta-carotene solution and the mixture was stirred at 50 ºC until complete evaporation of chloroform (around 10 minutes). After chloroform evaporation 50 mL of water, was added slowly, making sure that a clean emulsion was obtained. These mixture should be between the values of 0.6-0.7 in 470 nm.

A white solution was prepared using the previous description but substituting the beta-carotene solution to 50 mL of water.

Test solutions were prepared in DMSO in different dilutions and comprised 200 µl standard or sample + 800 µl of the beta-carotene/linoleic acid emulsion (in flakes), incubated in the dark at 50 ºC for 120 min and then read for absorbance at 470 nm. Three independent assays, each with a duplicate for the test samples and the appropriate solvent blank, were conducted.

4.2.9. DNA intercalation studies

For the DNA intercalation studies, 0.250 mg of DNA were dissolved in 10 mL of PBS in a volumetric flask to the control solution.

To the preparation of the solution DNA/**8b** (10:1) it was transferred 2.5 mL of DNA solution [1.51×10^{-4} M] to a 5 mL volumetric flask. After that, 2.45 mg of **5b** was dissolved in 10 mL of DMSO.

Finally, 2.5 mL of DNA solution and 0.1 mL of **8b** solution (3.8×10^{-8} mol) were transferred to a 5 mL volumetric flask and the volume was perfected to 5 mL of PBS.

The intercalation studies of the glycosylated pyrazole **6b** were performed by my colleague Ana, following the same procedure, and her results were used to compare with the results obtained for pyrazole **8b**.

4.2.10. 3-(4,5-dimethylthiazol-2-yl)-2,5-diphenyltetrazolium bromide (MTT) assay

Stock solutions of **2a**, **2b**, **4a**, **8a** and **8b** (20 mM) were prepared in DMSO. Stock solutions were diluted to obtain the test solutions at the required concentrations for the biological assays. In all the experiments, the highest concentration of DMSO in each well was 0.5% (v/v). MTT was prepared in PBS (5 mg mL^{-1}) and sterilized by filtration.

The Faculty of Pharmacy, University of Porto, kindly provided the human stomach gastric adenocarcinoma (AGS) and the human healthy lung fibroblasts (MRC-5) cell lines.

The two cell lines were grown in monolayers in 75 cm^2 tissue culture flasks at 37ºC in a humidified atmosphere with 5% of CO_2, sub-cultured every 3 days and harvested upon addiction of trypsin/EDTA (0.05% or 0.25% trypsin/EDTA solution). The culture mediums were DMEM (1X) + GlutaMAX^{TM-1} for AGS and MEM (1X) + GlutaMAX^{TM-1} for MRC-5, supplemented with 10% heat-inactivated fetal bovine serum (FBS), penicillin-streptomycin (100 units mL^{-1} penicillin and 100 µg mL^{-1} streptomycin).

Cell viability following exposure of the AGS and MRC-5 cells to test solutions with different concentrations of **2a**, **2b**, **4a, 8a** and **8b** was assessed at 24 hours of incubation. Each concentration was tested by three independent experiments with triplicates. AGS and MRC-5 cells were respectively plated at a density of 1.5×10^4 and 2.0×10^4 cells cm^{-2} in

96-well microplates. The test solutions were added 24 hours after seeding and incubated at 37 ℃. After 24 hours, 100 µL of MTT was added to each well, and the plates were incubated for 2h. Later, MTT was removed and the cells washed with 200 µL of DMSO/Isopropanol (3:1) under stirring to remove the purple formazan crystals. The optical density was measured in a microplate reader at 570 nm.

The statistical analysis of the results was performed using the software package *Prism*, by *GraphPad*. The t-student test was employed for a statistical comparison between the experimental data, p-values < 0.05 being deemed significant. The IC_{50} values were determined using nonlinear regression analysis, fitting the results in sigmoidal dose-response curves (variable slope).

5. Results and discussion

5.1. Antioxidant activity

The antioxidant activities of the pyrazoles **2a-d**; **6b** and **6d** were determined by following the reduction of ABTS$^{\cdot+}$, a blue-colored radical cation which turns colorless upon reduction. The percentage of inhibition of pyrazoles and standards was plotted as a function of the concentration of pyrazoles and standards. The IC_{50} value for each samples and standards were calculated with the statistical determinants (average, standard deviation and the percentage of error) and the results were compared in order to establish an attemptive structure-activity relationship. The results for the IC_{50} are presented on table 5.1 for each tested compound and the statistical comparison between all pyrazoles and standards on figure 5.2.

Compounds **9** and **10** were already available on the laboratory and were provided in order to evaluate the effect in radical scavenging activity of the substitution in the pyrazole ring.

1a: R=H
1b: R=Cl
1c: R=NO2
1d: R=OCH3

2a: R=H
2b: R=Cl

Ascorbic Acid (Vit. C)

α-tocopherol (Vit. E)

Figure 5.1 - Chemical structure of the pyrazole derivatives and standards (ascorbic acid and tocopherol) tested for antioxidant effect by following the decolorization (reduction) of ABTS$^{\cdot+}$ radical cation at 734 nm.

Table 5.1 – Antioxidant activity of pyrazole derivatives and standards, determined by the ABTS$^{\cdot+}$ assay through measuring the reduction of the radical cation as the percentage inhibition of absorbance at 734 nm. Data is presented as mean ± SD (middle column) and the associated error percentage (right column).

Compounds	IC_{50} (μM)	% Error
α-Tocopherol (a)	15.28±0.29	1.9
Ascorbic Acid (b)	10.56±0.69	6.5
2a	13.21±1.63	12.3
2b	22.99±0.72	3.1
2c	17.10±2.13	12.4
2d	15.80±2.01	12.7
4b	19.10±1.52	8.0
6	N.D	N.D
9	21.18±2.06	9.7
10	23.26±1.54	6.6
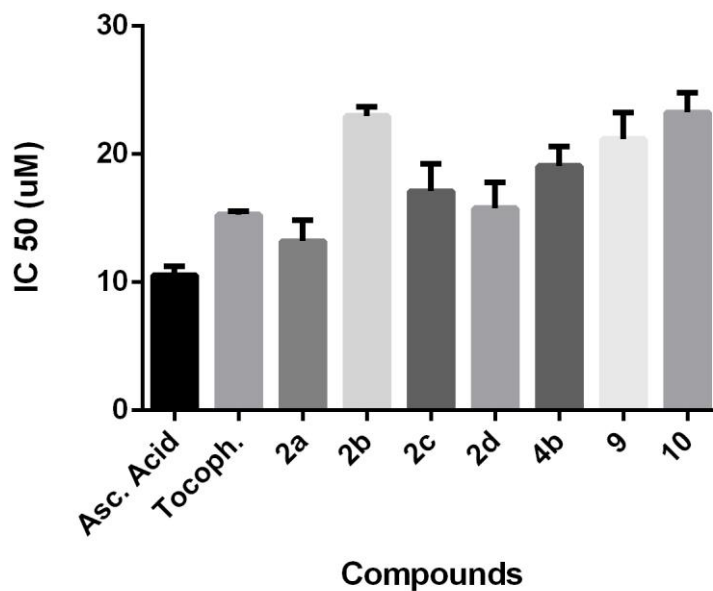
Figure 5.2 - ABTS$^{\cdot+}$ assay results of pyrazole derivatives, compared with ascorbic acid and tocopherol.

5.1.2. Structure-activity relationship

Looking at table 5.1 and Figure 5.2, we can see that for standards, ascorbic acid presented the best IC_{50} (10.56 µM) when compared with α-tocopherol (15.28 µM), meeting the results that were already described in the literature [54]. In general, the antioxidant effect of pyrazoles depends on the structure and the substitution pattern of the R group in position C-4''. The introduction of the α-glucose group by an ether linkage at 2'-OH position of compound **6,** presented insignificant antioxidant activity leading us to conclude that the presence of the hydroxyl group in the aromatic ring is an essential requirement for effective radical scavenging. Another essential requirement for antioxidant activity seems to be the free NH in the pyrazole ring once the insertion of a methyl group in compound **9** significantly increased the IC_{50} when compared with the non-substituted NH of **2a**. For pyrazole **10**, the increase of the IC_{50} value once again revealed the need of a free hydroxyl group in the aromatic ring. However, while the insertion of a methyl group (**9**) in the NH of the pyrazole ring showed significant differences for the IC_{50} values (from 13.21 (**2a**) to 21.18 µM), the difference between **9** and **10** was significantly lower (from 21.18 to 23.26 µM). This reveals that, besides OH has an important role on the antioxidant effect, the free NH of the pyrazole ring seems to be more essential to this mechanism.

The comparison between pyrazole isomers **2b** and **4b** among with their respective IC_{50} values (22.90 and 19.10 µM), revealed that the presence of the [2-(4-chlorophenyl)vinyl] at 4-position increases the radical scavenging ability, probably because allows a better delocalization and stabilization of the radical electron by resonance. In addition, to see the effect of R group in position C-4'' in the radical scavenging activity, the IC_{50} values of compounds with different R groups were compared and revealed interesting results. Looking at table 5.1 we can see that among pyrazoles **2**, **2a** presented the best radical scavenging activity with a value for IC_{50} (13.21 µM) between both standards ascorbic acid (10.56 µM) and α-tocopherol (15.28 µM). When comparing **2a** with **2b-d** we can notice that the presence of a substituent affects the radical scavenging ability, independently of the electronic nature of the substituent. However, the pyrazole **2d,** which has an electron-donating substituent (R = OCH_3) gave better results than **2b** and **2c**, with an IC_{50} of 15.8 µM (near to α-tocopherol). We believe that the presence of an electron-donor substituent

such as the methoxyl group in **2d** or the presence of an eletron with drawing substituent such as the nitro group (**2c**) are more prone to stabilize the radical due to resonance effects. Looking at table 3.1, pyrazole **2b** presented the worse value for radical scavenging ability. Knowing that **2b** is one of the most less soluble pyrazole among all **2** derivatives, we postulated that the solubility of the compound, which is a very important requisite for antioxidant tests by ABTS reduction method, could have any interference on the results obtained.

It should be noted that, in order to approach different antioxidant mechanisms, we also tried to study for NO scavenging and beta-carotene assays. However, these activities couldn't be accessed due to solubility issues of the pyrazoles.

Taking into account these results, we decided to choose compound **2a** and also **4a** (due to the strong antioxidant effect of **4b**) for cell cytotoxicity assays against tumor and healthy cell lines. However, considering that the mechanism of action for radical scavenging and for cytotoxicity is different, we also choose pyrazole **2b** in order to establish a relation beteween the structure (position of the styryl moiety) and biological activity.

5.2. Cytotoxic and cytostatic activity

5.2.1. 3-(4,5-dimethylthiazol-2-yl)-2,5-diphenyltetrazolium bromide (MTT) assay

The cytotoxicity of pyrazoles **2a**, **2b**, **4a** and of pyrazole-ruthenium(II) complexes **8a** and **8b** were evaluated against AGS cancer cell lines and healthy fibroblasts from MRC-5 cell lines.

Compounds **8a** and **8b** displayed the highest biological activity (Table 5.1 and Figure 5.3) against AGS with IC_{50} values of 11.26 and 11.02 µM, respectively, indicating that the introduction of a ruthenium(II)-tritiacyclonane complex in the pyrazole has an important role on cytotoxic activity. While previous studies demonstrated that [Ru([9]aneS3)(*php-OCH₃*)Cl₂] (**8d**) had a significant IC_{50} value for PC-3 and MDA-MB-231 cells (32.2 and 19.2 µM, respectively)[6], our study may have just revealed that [Ru([9]aneS3)(*phpz*)Cl₂] are probably more effective against AGS cells. To confirm this hypothesis further studies on AGS cells with pyrazole **8d** will be necessary.

Table 5.1 - Inhibition growth concentrations (IC_{50}) for pyrazoles derivatives **2a, 2b, 4a** and for pyrazole-ruthenium(II) complexes **8a** and **8b** against AGS and MRC-5, gaven by MTT assay and determined using nonlinear regression analysis, fitting the results in sigmoidal dose- response curves (variable slope) in GraphPad Prism.

| Compounds	IC_{50} AGS (24 h)	IC_{50} MRC-5 (24 h)
2a	25.44	n.d
2b	24.84	n.d
4a	24.92	n.d
8a	11.26	28.29
8b	11.02	28.45
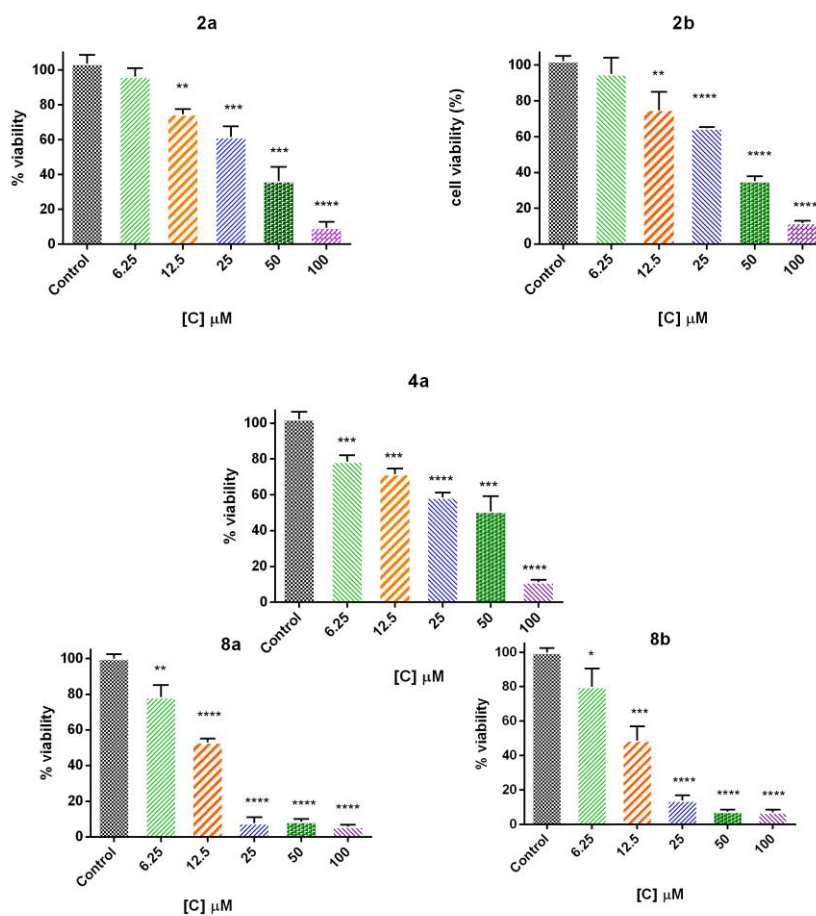
Figure 5.3 - Cytotoxic effect of the compounds **2a**, **2b**, **4a**, **8a** and **8b** at different concentrations and after 72h of incubation on the human stomach cancer line AGS .The data are expressed as a percentage of

the control (100%) and represent the average ± mean standard deviation from experiments carried out in triplicate; * denotes *p*-value < 0.05; ** denotes *p*-value < 0.001; **** denotes *p*-value < 0.0001.

Previous studies also revealed the cytotoxicity of **2d** against PC-3 and MDA-MB-231 cells with the respective values for IC_{50} of 9.9 and 10.2 µM[6]. Our study, due to the respective IC_{50} for both **2a** and **2b** of 25.44 and 24.84 µM (table 4.1) shows us that *phpz* derivatives are probably worse candidates for AGS than for PC-3 and MDA-MB-231 cells. However to confirm our suspicion further studies on AGS cells with pyrazole **2d** are necessary.

The IC_{50} values were determined using nonlinear regression analysis, fitting the results in sigmoidal dose-response curves (variable slope) (see figure 5.4).
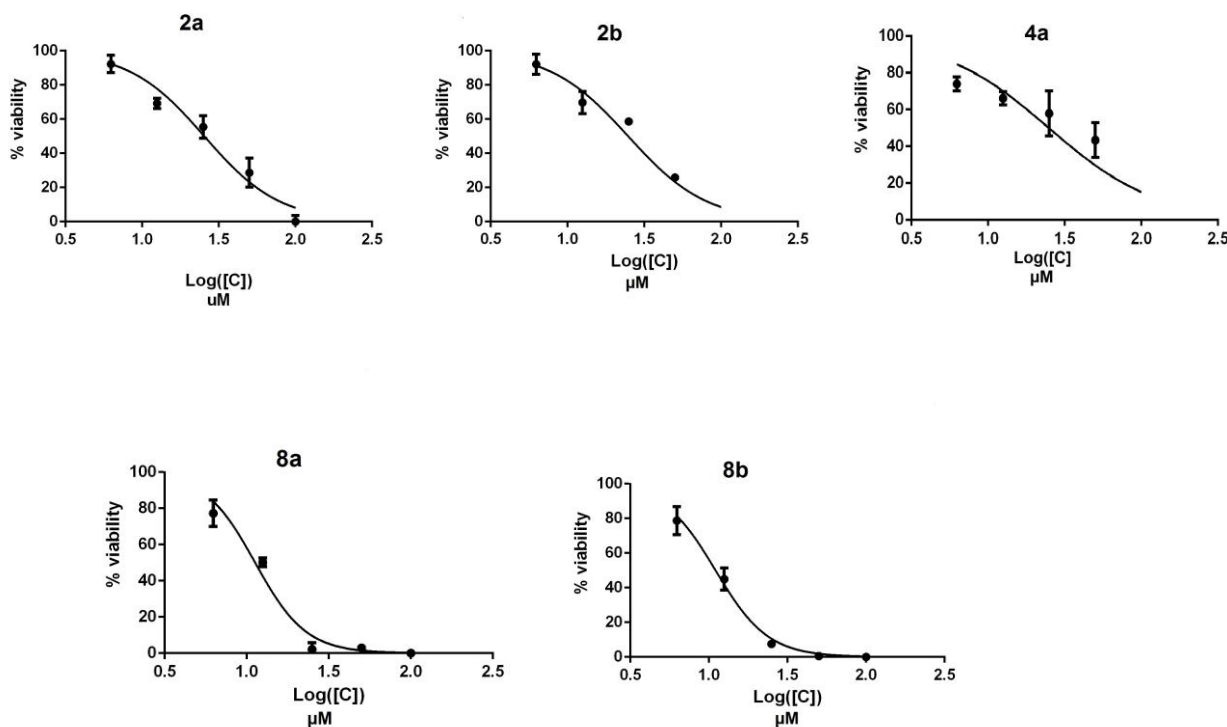
Figure 5.4 - Results for the nonlinear regression analysis of the percentage of viability of AGS for different concentrations of all the tested compounds, using MTT assay and sub-cultivation of cells every 3 days.
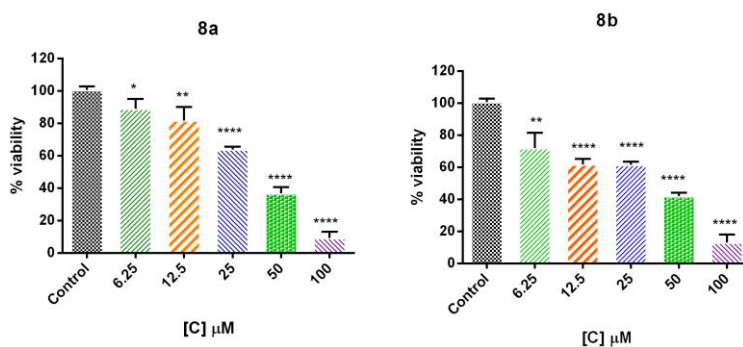
5.2.1.1. Structure-Activity Relationship

Just like in the antioxidant effect studies, structure-activity relationships between pyrazoles have been considered. Looking at table 5.2 we can see that between pyrazole **2a** and pyrazole **4a**, the differences between their IC_{50} are almost insignificant (25.44 and 24.92 µM, respectively). Thus, unlike the results obtained for the ABTS assay, here the position of the styryl moiety did not have significant interference in the cytotoxic activity. Furthermore, the comparison between pyrazoles **2a** and **2b** or between the ruthenium(II) complexes **8a** and **8b**, which presented similar values for IC_{50} (see table 5.2), indicates that the presence of a Cl group at 4"-position of the phenyl ring has no significant effect in the cytotoxicity of pyrazoles.

Noteworthy that the introduction of a ruthenium complex increased the cytotoxicity of pyrazoles, allowing us to conclude that the complex displays an important role in the biologic activity.

5.2.1.2. Toxicity on healthy cells

In order to understand if pyrazoles and ruthenium complexes feature selective action against tumoral cells, we also tested the cytotoxicity on a healthy lung fibroblast cell line (MRC-5). Unfortunately, because the proliferation behavior of non-cancer cells is slower, there was not enough time to evaluate the toxicity of free pyrazoles. We believe that this could also be due to the ageing of MRC-5 cells that weren't proliferating in a healthy way anymore.
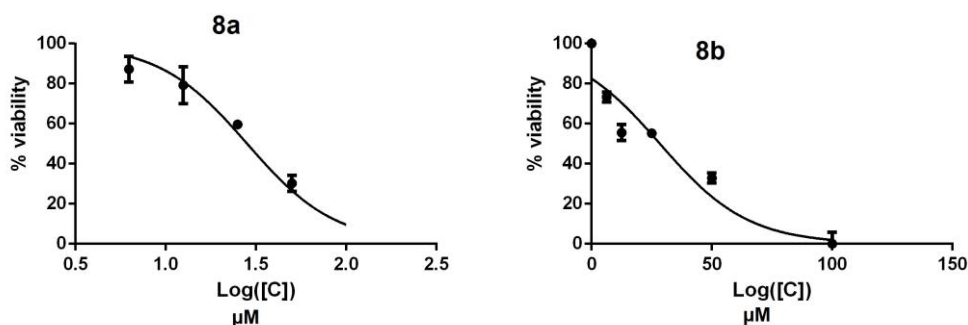
Cytotoxicity against MRC-5

The IC_{50} values were determined using nonlinear regression analysis, fitting the results in sigmoidal dose- response curves of variable slope (figure 5.6).

Figure 5.6 - Results for the nonlinear regression analysis of the percentage of viability of MRC-5 at different concentrations of compounds **8a** and **8b**, using MTT assay and cell sub-cultivation every 3 days.

The results obtained for the ruthenium complexes are represented in the table 5.1.

Overall the IC_{50} values on the healthy cells are higher than those determined for the tumoural cell line, by almost three-fold. This result, albeit positive, denotes a short safety margin. However, more tests should be done before further conclusions can be drawn. Testing the ruthenium complexes against non-cancer stomach cells could be a possible approach, since lung fibroblasts are usually more resistant cells. In addition, the compounds **2** and **4** need also to be evaluated to understand if free pyrazoles may display selective action.

5.2.2. DNA intercalation study – Cytostatic activity

The study of DNA intercalation is very important to understand cytostatic activity by pyrazoles. The cell, in order to replicate, must proceed to the replication of its own DNA. By an intercalation from new molecules, the machinery of cellular replication it is compromised.

Ruthenium complex **8b** was tested for DNA intercalation by studying the DNA melting point and compared to the one already studied by Ana Carreira **6b** (Figure 5.7 and Figure 5.8), in the curricular unit of master project.
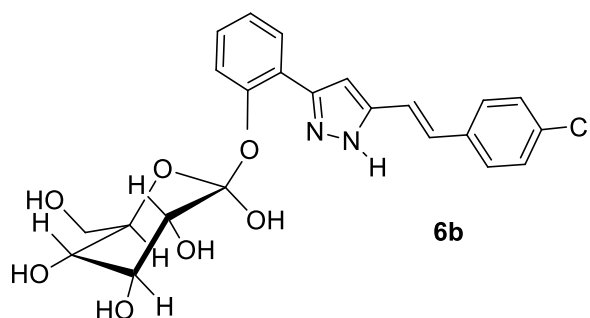
Figure 5.7 – Structure of the compound **6b**, studied by Ana Carreira for DNA intercalation.
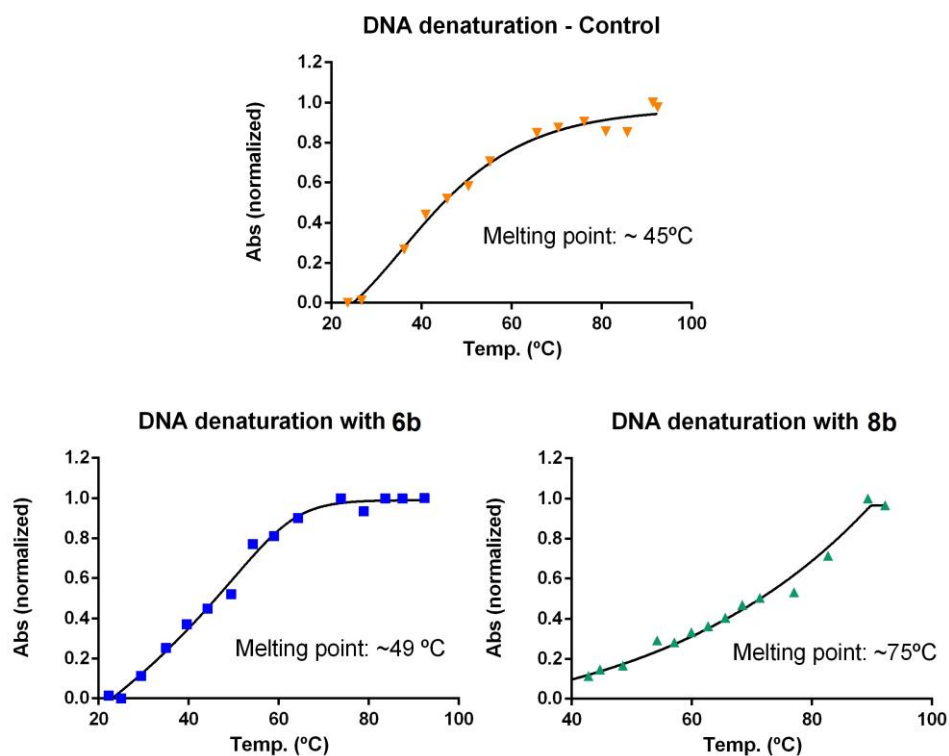
Figure 5.8– Denaturation curves of the solutions DNA (control), DNA + **6b** and DNA + **8b** in PBS (10:1), represented by the variation of normalized absorbance at 260 nm in function of temperature increase.

Looking at figure 5.7 we can see that **8b** presented the highest increase of DNA melting point. These results indicate that the insertion of a ruthenium group has more impact on the DNA intercalation than a glucose monomer. However, according to the literature, an increase of 2 ℃ in an indicator of an intercalative interaction type. For that reason, we can conclude that both **6b** and **8b** presented this type of intercalation against DNA.

6. Conclusions and future perspectives

The present work aimed at evaluating the biological activity of pyrazole derivatives, followed by their glycosylation and incorporation into ruthenium (II) complexes and structure-activity relationship studies.

The focus was to obtain a new compound with antioxidant and antitumoral activity, with possible selectivity for cancer cells and promising smoother treatment for cancer.

Given the link between cancer and oxidative stress, the drug candidates were first evaluated for their antioxidant activity. Compounds of family **2a-d** and compounds **4b** and **6a** were tested by the ABTS scavenging assay. The tests suggested that the presence of the pyrazole ring is several important in the radical scavenging and that the introduction of a glucose monomer does not positively affect this mechanism. Moreover, the comparison between pyrazole **2b** and **4b** showed that **4b** is a better radical scavenger, making us conclude that a 4-(phenyl)-vinyl design increases the radical scavenging ability. Last, from all pyrazoles of family **2**, pyrazole **2a** showed to be the best antioxidant, which may imply that the introduction of a receptor/donor group probably destabilizes the delocalization of the radical electron to the nucleus. The antioxidant test for beta-carotene was also carried out, but no significant results were obtained, leading to the conclusion that the antioxidant mode of action of these pyrazoles is associated more with radical scavenging action rather than protection of beta-carotene.

The cytotoxicity activity of pyrazoles was tested by using the MTT colorimetric assay for cancer cell lines of the stomach (AGS) and healthy fibroblasts of the lung (MRC-5). Pyrazoles **8a** and **8b** presented a highest cytotoxicity against AGS when compared to pyrazoles **2a** and **2b**, showing that the ruthenium(II) complex have significant effect on killing cells. The toxicity of these compounds on healthy tissue is not yet totally evaluated and it is not possible yet to recognize the best option for a possible smooth treatment of cancer. Glycopyrazoles (family **6**) must also be tested in order to understand if the glucose monomer affects the cytotoxicity and the selectivity for cancer cell lines.

The cytostatic activity of pyrazole **8b** was tested by studying its DNA intercalation ability and compared to the one already obtained for glycopyrazole **6b**. These studies revealed that the new ruthenium complex **8b** have a higher intercalation power that the

one glycosylated **6b**. However, several more studies must be made in order to also understand the intercalation power of free *phpz*.

Several tests are still important to do in the continuation of this work to achieve a better understanding of what kind of skeleton can be a better option for cancer patient-friendly treatment. To know the exact mechanism of action for cytotoxicity is one of our future proposals, as so to test the pyrazoles against other types of cell lines and also to increment glycopyrazoles in the cytotoxicity tests.

The results for this present work make us to consider that ruthenium complex **8b** is a promising compound to use in cancer chemotherapy due to its cytotoxicity and cytostatic properties. Indeed, most of the clinic antitumoral drugs are based on cytostatic action, that is, the ability to stop cancer cell replication. However, the cytotoxicity against healthy fibroblasts of the lung showed that **8b** has a small safety margin and thus it may have side effects when used *in vivo*. The results herein obtain are thus still not fully compliant with the goal of discovering an entirely new compound capable of reducing the side effects caused by chemotherapy. The future search for this agent may start by evaluating the cytotoxicity of glycosylated pyrazoles among with their selectivity for cancer cell lines. Secondly, should the glycation strategy prove successful, the preparation of a glycated analogue of **6b** would be interesting, in order to use the sugar monomer as a bait for cancer cells.

The antioxidant effect of ruthenium (II) complexes was not tested, because the ABTS assay suggested that the presence of free pyrazole ring is several important in the radical scavenging as so the presence of the hydroxyl group. For that reason, the expected new glycosylated **8b** could not be able to act as antitumoral and antioxidant at the same time. However, such pyrazoles as **2a** and **4b** presented high radical scavenging activity, which encourage us one more time to study the selectivity for cancer cell lines of family **2** and **4** and who knows to find a non-side effect antioxidant compound capable of reducing cancer probability by acting on chronic inflammation sites.

Finally, we also consider that the cytotoxicity of pyrazoles **2** and **4** may be related to their antioxidant activity as well, due to the fact that cancer has an incredible oxidant environment and the action of pyrazole can possibly fight the damage caused by oxidation.

ANNEXES

ANNEX 1:

(*E*)-3(5)-(2-hydroxyphenyl)-5(3)-styryl-1*H*-pyrazole (2a)

¹H NMR (300.13 MHz, CDCl$_3$): δ(ppm) = 6.78 (s, 1 H, 4-H), 6.94 (dt, *J* = 7.6, 1.2 Hz, 1 H, 5'- H), 6.98 (d, *J* = 16.5 Hz, 1 H, H-α), 7.04 (dd, *J* = 8.0, 1.2 Hz, 1 H, 3'-H), 7.12 (d, *J* = 16.5 Hz, 1 H, H-β), 7.24 (ddd, *J* = 7.6, 8.0, 1.6 Hz, 1H, 4'-H), 7.32 (tt, *J* = 7.1, 1.3 Hz, 1 H, 4''-H), 7.40 (dd, *J* = 8.4, 7.1 Hz, 2 H, 3'',5''-H), 7.51 (dd, *J* = 8.4, 1.3 Hz, 2 H, 2'',6''-H); 7.61 (dd, *J* = 7.6, 1.6 Hz, 1 H, 6'-H), 10.10 (br. s, 1 H, NH), 10.78 (br. s, 1 H, 2'-OH), see labeling scheme below [51].

¹³C NMR (75.47MHz, CDCl$_3$)**:** δ (ppm) = 99.7 (C'4), 114.3 (C-α), 116.4 (C-1'), 117.1 (C-3'), 119.4 (C-5'), 126.5 (C-6'), 126.7 (C-2'',6''), 128.7 (C-4''), 128.9 (C-3'',5''), 129.4 (C-4'), 132.2 (C-β), 135.8 (C-1''), 142.0 (C-5), 152.9 (C-3), 155.9 (C-2') [51].
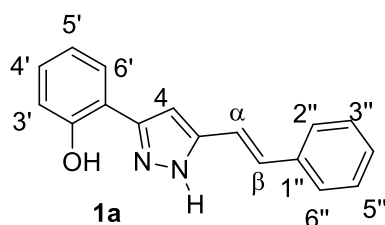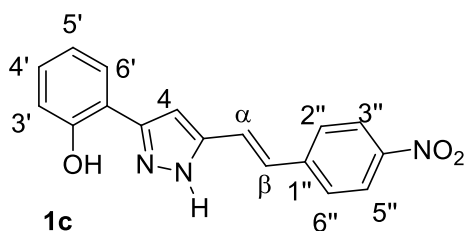

Annex 1a - Atom labelling scheme for compound **2a**

(*E*)-3(5)-(2-hydroxyphenyl)-5(3)-[2-(4-nitrophenyl)vinyl]-1*H*-pyrazole (2c)

¹H NMR (300.13 Hz, CDCl₃): δ(ppm) = 6.93 (ddd, *J* = 7.8, 7.6, 1.0 Hz, 1 H, 5'-H), 6.95 (dd, *J* = 8.0, 1.0 Hz, 1 H, 3'-H), 7.19 (s, 1 H, 4-H), 7.22 (ddd, *J* = 8.0, 7.6, 1.6 Hz, 1 H, 4'-H), 7.52 (s, 2 H, H-α and H-β), 7.74 (dd, *J* = 7.8, 1.6 Hz, 1 H, 6'-H), 7.89 (d, *J* = 7.0 Hz, 2 H, 2'',6''-H), 8.28 (d, *J* = 7.0 Hz, 2 H, 3'',5''-H), 10.79 (br. s, 1 H, NH), 12.81 (br. s, 1 H, 2'-OH) ppm.

¹³C NMR (75.47 MHz, CDCl₃): δ (ppm) = 101.4 (C- 4), 117.4 (C-1'), 117.5 (C-3'), 120.1 (C-5'), 124.9 (C-3'',5''), 127.5 (C-6'), 128.2 (C-2'',6''), 130.0 (C-4'), 130.5 (C-α and C-β), 142.0 (C-1''), 143.1 (C-5), 146.6 (C-4''), 148.1 (C-3), 156.9 (C-2')[51]

Annex 1b - Atom labelling scheme for compound **2c**

(*E*)-3(5)-(2-hydroxyphenyl)-5(3)-[2-(4-methoxyphenyl)vinyl]-1*H*-pyrazole (2d)

¹H NMR (300.13 Hz, CDCl₃): δ(ppm) = 3.84 (s, 3 H, 4''-OCH₃), 6.76 (s, 1 H, 4-H), 6.83 (d, *J* = 16.6 Hz, 1 H, H-α), 6.92 (d, *J* = 8.8 Hz, 2 H, 3'',5''-H), 6.93 (ddd, *J* = 8.2, 7.3, 1.2 Hz, 1 H, 5'-H), 7.04 (dd, *J* = 8.4, 1.2 Hz, 1 H, 3'-H), 7.05 (d, *J* = 16.6 Hz, 1 H, H-β), 7.24 (dt, *J* = 8.2, 1.6 Hz, 1 H, 4'-H), 7.44 (d, *J* = 8.8 Hz, 2H, 2'',6''- H), 7.60 (dd, *J* = 7.3, 1.6 Hz, 1 H, 6'-H), 10.04 (br. s, 1 H, NH), 10.83 (br. s, 1 H, 2'-OH) ppm.

¹³C NMR (75.47 MHz, CDCl₃): δ (ppm) = 55.4 (4''-OCH₃), 99.2 (C-4), 112.1 (C-α), 114.3 (C-3'',5''), 116.5 (C-1'), 117.1 (C- 3'), 119.3 (C-5'), 126.5 (C-6'), 128.0 (C-2'',6''), 128.6 (C-1''), 129.4 (C-4'), 131.8 (C-β), 142.3 (C-5), 152.9 (C-3), 160.1 (C-4''), 156.0 (C-2').[51]

1d
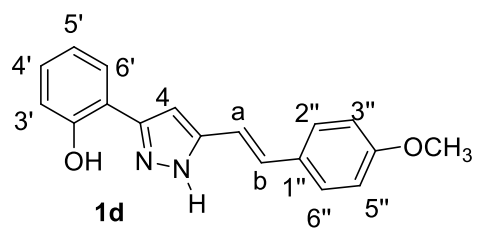
Annex 1c - Atom labelling scheme for compound **2d**

References

[1]   A. Araújo, F. Barata, S. Barroso, P. Cortes, M. Damasceno, A. Parreira, J. Espírito Santo, E. Teixeira, and R. Pereira, "Custo do tratamento do cancro em Portugal," *Acta Med. Port.*, vol. 22, no. 5, pp. 525–536, 2009.

[2]   S. A. F. Rostom, "Polysubstituted pyrazoles, part 6. Synthesis of some 1-(4-chlorophenyl)-4-hydroxy-1H-pyrazol-3-carbonyl derivatives linked to nitrogenous heterocyclic ring systems as potential antitumor agents," *Bioorganic Med. Chem.*, vol. 18, no. 7, pp. 2767–2776, 2010.

[3]   P. G. Baraldi, P. Cozzi, C. Geroni, N. Mongelli, R. Romagnoli, and G. Spalluto, "Novel benzoyl nitrogen mustard derivatives of pyrazole analogues of distamycin A: Synthesis and antileukemic activity," *Bioorganic Med. Chem.*, vol. 7, no. 2, pp. 251–262, 1999.

[4]   G. Daidone, B. Maggio, D. Raffa, S. Plescia, D. Schillaci, and M. V. Raimondi, "Synthesis and in vitro antileukemic activity of new 4-triazenopyrazole derivatives," *Farmaco*, vol. 59, no. 5, pp. 413–417, 2004.

[5]   T. Yamamoto, "Over-Expression of Facilitative Glucose Transporter Genes in Jiuman Cancer," *Biochem. Biophys. Res. Commun.*, vol. 170, pp. 223–230, 1990.

[6]   J. Marques, V. L. M. Silva, A. M. S. Silva, M. P. M. Marques, and S. S. Braga, "Ru(II) trithiacyclononane 5-(2-hydroxyphenyl)-3-[(4-methoxystyryl)pyrazole], a complex with facile synthesis and high cytotoxicity against PC-3 and MDA-MB-231 cells," *Complex Met.*, vol. 1, no. 1, pp. 7–12, 2014.

[7]   A. C. Society, "Do we know what causes prostate cancer?," 2016. [Online]. Available: http://www.cancer.org/cancer/prostatecancer/detailedguide/prostate-cancer-what-causes. [Accessed: 28-Jan-2016].

[8]   M. L. Macheda, S. Rogers, and J. D. Best, "Molecular and cellular regulation of glucose transporter (GLUT) proteins in cancer," *J. Cell. Physiol.*, vol. 202, no. 3, pp. 654–662, 2005.

[9]   S. I. Grivennikov, F. R. Greten, and M. Karin, "Immunity, Inflammation, and Cancer," *Cell*, vol. 140, no. 6, pp. 883–899, 2011.

[10] L. M. Coussens and Z. Werb, "Inflammation and cancer," *Nature*, vol. 420, pp. 860–867, 2002.

[11] E. A. Platz and A. M. D. E. Marzo, "Epidemiology of inflammation and prostate cancer," vol. 171, no. February, pp. 36–40, 2004.

[12] G. T. MacLennan, R. Eisenberg, R. L. Fleshman, J. M. Taylor, P. Fu, M. I. Resnick, and S. Gupta, "The influence of chronic inflammation in prostatic carcinogenesis: a 5-year followup study.," *J. Urol.*, vol. 176, no. 3, pp. 1012–1016, 2006.

[13] G. M. Nitulescu, C. Draghici, O. T. Olaru, L. Matei, A. Ioana, L. D. Dragu, and C. Bleotu, "Synthesis and apoptotic activity of new pyrazole derivatives in cancer cell lines," *Bioorganic Med. Chem.*, vol. 23, no. 17, pp. 5799–5808, 2015.

[14] H. Kumar, D. Saini, S. Jain, and N. Jain, "Pyrazole scaffold: A remarkable tool in the development of anticancer agents," *Eur. J. Med. Chem.*, vol. 70, pp. 248–258, 2013.

[15] R. Lin, G. Chiu, Y. Yu, P. J. Connolly, S. Li, Y. Lu, M. Adams, A. R. Fuentes-Pesquera, S. L. Emanuel, and L. M. Greenberger, "Design, synthesis, and evaluation of 3,4-disubstituted pyrazole analogues as anti-tumor CDK inhibitors," *Bioorganic Med. Chem. Lett.*, vol. 17, no. 16, pp. 4557–4561, 2007.

[16] E. L. Mayer, "Targeting Breast Cancer with CDK Inhibitors," *Curr. Oncol. Rep.*, vol. 17, no. 5, pp. 15–19, 2015.

[17] R. Lin, P. J. Connolly, Y. Lu, G. Chiu, S. Li, Y. Yu, S. Huang, X. Li, S. L. Emanuel, S. A. Middleton, R. H. Gruninger, M. Adams, A. R. Fuentes-Pesquera, and L. M. Greenberger, "Synthesis and evaluation of pyrazolo[3,4-b]pyridine CDK1 inhibitors as anti-tumor agents," *Bioorganic Med. Chem. Lett.*, vol. 17, no. 15, pp. 4297–4302, 2007.

[18] S. Huang, R. Lin, Y. Yu, Y. Lu, P. J. Connolly, G. Chiu, S. Li, S. L. Emanuel, and S. A. Middleton, "Synthesis of 3-(1H-benzimidazol-2-yl)-5-isoquinolin-4-ylpyrazolo[1,2-b]pyridine, a potent cyclin dependent kinase 1 (CDK1) inhibitor," *Bioorganic Med. Chem. Lett.*, vol. 17, no. 5, pp. 1243–1245, 2007.

[19] A. Kinases and C. Cycle, "Aurora kinases : Structure , functions and their association with cancer," *Biomed Pap Med Fac Univ Palacky Olomouc Czech*

Repub., vol. 152, no. 1, pp. 27–33, 2008.

[20] D. Fancelli, J. Moll, M. Varasi, R. Bravo, R. Artico, D. Berta, S. Bindi, A. Cameron, I. Candiani, P. Cappella, P. Carpinelli, W. Croci, B. Forte, M. L. Giorgini, J. Klapwijk, A. Marsiglio, E. Pesenti, M. Rocchetti, F. Roletto, D. Severino, C. Soncini, P. Storici, R. Tonani, P. Zugnoni, and P. Vianello, "1,4,5,6-Tetrahydropyrrolo[3,4-c]pyrazoles: Identification of a potent aurora kinase inhibitor with a favorable antitumor kinase inhibition profile," *J. Med. Chem.*, vol. 49, no. 24, pp. 7247–7251, 2006.

[21] S.-F. Wang, Y.-L. Zhu, P.-T. Zhu, J. A. Makawana, Y.-L. Zhang, M.-Y. Zhao, P.-C. Lv, and H.-L. Zhu, "Design, synthesis and biological evaluation of novel 5-phenyl-1H-pyrazole derivatives as potential BRAFV600E inhibitors," *Bioorg. Med. Chem.*, vol. 22, no. 21, pp. 6201–6208, 2014.

[22] Q. S. Li, X. H. Lv, Y. Bin Zhang, J. J. Dong, W. P. Zhou, Y. Yang, and H. L. Zhu, "Identification of novel 3,5-diarylpyrazoline derivatives containing salicylamide moiety as potential anti-melanoma agents," *Bioorganic Med. Chem. Lett.*, vol. 22, no. 21, pp. 6596–6601, 2012.

[23] G. T. Gibney, J. L. Messina, I. V Fedorenko, V. K. Sondak, and K. S. M. Smalley, "Paradoxical oncogenesis--the long-term effects of BRAF inhibition in melanoma," *Nat. Rev. Clin. Oncol.*, vol. 10, no. 7, pp. 390–399, 2013.

[24] A. R. McCarthy, L. Pirrie, J. J. Hollick, S. Ronseaux, J. Campbell, M. Higgins, O. D. Staples, F. Tran, A. M. Z. Slawin, S. Lain, and N. J. Westwood, "Synthesis and biological characterisation of sirtuin inhibitors based on the tenovins," *Bioorganic Med. Chem.*, vol. 20, no. 5, pp. 1779–1793, 2012.

[25] B. J. Ryu, M. K. Hwang, M. Park, K. Lee, and S. H. Kim, "Thiourea compound AW00178 sensitizes human H1299 lung carcinoma cells to TRAIL-mediated apoptosis," *Bioorganic Med. Chem. Lett.*, vol. 22, no. 12, pp. 3862–3865, 2012.

[26] S. Xanthoudakis and D. W. Nicholson, "Heat-shock proteins as death determinants.," *Nat. Cell Biol.*, vol. 2, no. 9, pp. E163–E165, 2000.

[27] P. A. Brough, X. Barril, M. Beswick, B. W. Dymock, M. J. Drysdale, L. Wright, K. Grant, A. Massey, A. Surgenor, and P. Workman, "3-(5-chloro-2,4-dihydroxyphenyl)-Pyrazole-4-carboxamides as inhibitors of the Hsp90 molecular

chaperone," *Bioorganic Med. Chem. Lett.*, vol. 15, no. 23, pp. 5197–5201, 2005.

[28] S. Grosse, V. Mathieu, C. Pillard, S. Massip, M. Marchivie, C. Jarry, P. Bernard, R. Kiss, and G. Guillaumet, "New imidazo[1,2-b]pyrazoles as anticancer agents: Synthesis, biological evaluation and structure activity relationship analysis," *Eur. J. Med. Chem.*, vol. 84, pp. 718–730, 2014.

[29] D. Dreher and A. F. Junod, "Role of oxygen free radicals in cancer development.," *Eur. J. Cancer*, vol. 32A, no. 1, pp. 30–38, 1996.

[30] K. B. Umesha, K. M. L. Rai, and M. A. H. Nayaka, "Antioxidant and Antimicrobial Activity of 5-methyl-2-," vol. 5, no. 4, pp. 359–368, 2009.

[31] P. Gurunanjappa and A. K. Kariyappa, "Design, synthesis and biological evaluation of 1,3,4-oxadiazoles/thiadiazoles bearing pyrazole scaffold as antimicrobial and antioxidant candidates," *Curr. Chem. Lett.*, vol. 5, pp. 109–122, 2016.

[32] Y. F. Li and Z. Q. Liu, "Dendritic antioxidants with pyrazole as the core: Ability to scavenge radicals and to protect DNA," *Free Radic. Biol. Med.*, vol. 52, no. 1, pp. 103–108, 2012.

[33] R. N. Dubois, S. B. Abramson, L. Crofford, R. A. Gupta, L. S. Simon, L. B. Van De Putte, and P. E. Lipsky, "Cyclooxygenase in biology and disease.," *FASEB J.*, vol. 12, no. 12, pp. 1063–1073, 1998.

[34] R. D. Kamble, R. J. Meshram, S. V. Hese, R. A. More, S. S. Kamble, R. N. Gacche, and B. S. Dawane, "Synthesis and in silico investigation of thiazoles bearing pyrazoles derivatives as anti-inflammatory agents," *Comput. Biol. Chem.*, vol. 61, pp. 86–96, 2016.

[35] D. F. Hildebrand, "What ' s New in Plant Physiology Lipoxygenases," *Physiol. Plantarium*, vol. 76, pp. 249–253, 1989.

[36] M. a-a El-Sayed, N. I. Abdel-Aziz, A. a-M. Abdel-Aziz, A. S. El-Azab, Y. a Asiri, and K. E. H. Eltahir, "Design, synthesis, and biological evaluation of substituted hydrazone and pyrazole derivatives as selective COX-2 inhibitors: Molecular docking study.," *Bioorg. Med. Chem.*, vol. 19, no. 11, pp. 3416–3424, 2011.

[37] T. Kawamori, C. V. Rao, K. Seibert, and B. S. Reddy, "Chemopreventive activity of celecoxib, a specific cyclooxygenase-2 inhibitor, against colon carcinogenesis,"

Cancer Res., vol. 58, no. 3, pp. 409–412, 1998.

[38]   S. G. Alegaon, M. B. Hirpara, K. R. Alagawadi, K. K. Hullatti, and K. Kashniyal, "Synthesis of novel pyrazole-thiadiazole hybrid as potential potent and selective cyclooxygenase-2 (COX-2) inhibitors.," *Bioorg. Med. Chem. Lett.*, vol. 24, no. 22, pp. 5324–5329, 2014.

[39]   B. Pelcman, A. Sanin, P. Nilsson, W. Schaal, K. Olofsson, C. Krog-Jensen, P. Forsell, A. Hallberg, M. Larhed, T. Boesen, H. Kromann, and H. E. Claesson, "N-Substituted pyrazole-3-carboxamides as inhibitors of human 15-lipoxygenase," *Bioorganic Med. Chem. Lett.*, vol. 25, no. 15, pp. 3017–3023, 2015.

[40]   J. Hu, W. Zhu, H. Meng, Y. Liu, X. Wang, and C. Hu, "Identification of 1, 4-Dihydrothieno[3′, 2′:5, 6]thiopyrano[4, 3-c]pyrazole Derivatives as Human 5-Lipo-oxygenase Inhibitors," *Chem. Biol. Drug Des.*, vol. 84, no. 6, pp. 642–647, 2014.

[41]   A. Bergamo, C. Gaiddon, J. H. M. Schellens, J. H. Beijnen, and G. Sava, "Approaching tumour therapy beyond platinum drugs: Status of the art and perspectives of ruthenium drug candidates," *J. Inorg. Biochem.*, vol. 106, no. 1, pp. 90–99, 2012.

[42]   B. C. S. Allardyce and P. J. Dyson, "Ruthenium in Medicine : Current Clinical Uses and Future Prospects," *Platin. Met. Rev.*, vol. 45, no. 2, pp. 62–69, 2001.

[43]   G. Sava, I. Capozzi, K. Clerici, G. Gagliardi, E. Alessio, and G. Mestroni, "Pharmacological control of lung metastases of solid tumours by a novel ruthenium complex," *Clin. Exp. Metastasis*, vol. 16, no. 4, pp. 371–379, 1998.

[44]   G. Sava, S. Zorzet, C. Turrin, F. Vita, M. Soranzo, G. Zabucchi, M. Cocchietto, A. Bergamo, S. Digiovine, G. Pezzoni, and L. Sartor, "Dual Action of NAMI-A in Inhibition of Solid Tumor Metastasis : Selective Targeting of Metastatic Cells and Binding to Collagen Dual Action of NAMI-A in Inhibition of Solid Tumor Metastasis : Selective Targeting of Metastatic Cells and Binding to Collagen," *Clin. Cancer Res.*, vol. 9, no. May, pp. 1898–1905, 2003.

[45]   G. Sava, S. Zorzet, C. Turrin, F. Vita, M. Soranzo, G. Zabucchi, M. Cocchietto, A. Bergamo, S. Digiovine, G. Pezzoni, and L. Sartor, "Dual Action of NAMI-A in Inhibition of Solid Tumor Metastasis : Selective Targeting of Metastatic Cells and Binding to Collagen Dual Action of NAMI-A in Inhibition of Solid Tumor

Metastasis : Selective Targeting of Metastatic Cells and Binding to Collagen," *Clin. Cancer Res.*, vol. 9, pp. 1898–1905, 2003.

[46]   G. Sava, F. Frausin, M. Cocchietto, F. Vita, E. Podda, P. Spessotto, A. Furlani, V. Scarcia, and G. Zabucchi, "Actin-dependent tumour cell adhesion after short-term exposure to the antimetastasis ruthenium complex NAMI-A," *Eur. J. Cancer*, vol. 40, no. 9, pp. 1383–1396, 2004.

[47]   S. Kapitza, M. A. Jakupec, M. Uhl, B. K. Keppler, and B. Marian, "The heterocyclic ruthenium(III) complex KP1019 (FFC14A) causes DNA damage and oxidative stress in colorectal tumor cells," *Cancer Lett.*, vol. 226, no. 2, pp. 115–121, 2005.

[48]   F. Lentz, A. Drescher, A. Lindauer, M. Henke, R. a Hilger, C. G. Hartinger, M. E. Scheulen, C. Dittrich, B. K. Keppler, and U. Jaehde, "Pharmacokinetics of a novel anticancer ruthenium complex (KP1019, FFC14A) in a phase I dose-escalation study.," *Anticancer. Drugs*, vol. 20, no. 2, pp. 97–103, 2009.

[49]   C. Scolaro, A. B. Chaplin, C. G. Hartinger, A. Bergamo, M. Cocchietto, B. K. Keppler, G. Sava, and P. J. Dyson, "Tuning the hydrophobicity of ruthenium(II)-arene (RAPTA) drugs to modify uptake, biomolecular interactions and efficacy.," *Dalton Trans.*, vol. 2, pp. 5065–5072, 2007.

[50]   B. J. Goodfellow, V. Félix, S. M. D. Pacheco, J. P. de Jesus, and M. G. B. Drew, "Structural characterisation of RuII [9]aneS3 polypyridyl complexes by NMR spectroscopy and single crystal X-ray diffraction," *Polyhedron*, vol. 16, no. 3, pp. 393–401, 1997.

[51]   V. L. M. Silva, A. M. S. Silva, D. C. G. A. Pinto, J. A. S. Cavaleiro, and J. Elguero, "3(5)-(2-Hydroxyphenyl)-5(3)-styrylpyrazoles: Synthesis and diels - Alder transformations," *European J. Org. Chem.*, vol. 3, no. 21, pp. 4348–4356, 2004.

[52]   V. L. M. Silva, A. M. S. Silva, D. C. G. a. Pinto, J. a. S. Cavaleiro, and J. Elguero, "Synthesis of (E)- and (Z)-3(5)-(2-hydroxyphenyl)-4-styrylpyrazoles," *Monatshefte für Chemie - Chem. Mon.*, vol. 140, no. 1, pp. 87–95, Sep. 2008.

[53]   M. Joana, V. Silva, A. Silva, P. M. Marques, and S. Braga, "Ru(II) trithiacylclononane 5-(2-hydroxyphenyl)-3-[(4-methoxystyryl)pyrazole], a complex with facile synthesis and high cytotoxicity against PC-3 and MDA-MB-231 cells,"

Complex Met., 2013.

[54]   R. Re, N. Pellegrini, a. Proteggente, a. Pannala, M. Yang, and C. Rice-Evans, "Antioxidant Activity Applying an Improved Abts Radical Cation Decolorization Assay," *Free Radic. Biol. Med.*, vol. 26, no. 9, pp. 1231–1237, 1999.

[ATCC] American Type Culture Collection (ATCC®), "PC-3 (ATCC® CRL-1435™)" [Online]. Available: http://www.lgcstandards-atcc.org/products/all/CRL-1435.aspx?geo_country=pt#characteristics